Multivalent Ligand–Receptor Binding Interactions in the Fibroblast Growth Factor System Produce a Cooperative Growth Factor and Heparin Mechanism for Receptor Dimerization

Michael W. Pantoliano,* Robert A. Horlick, Barry A. Springer, Drew E. Van Dyk, Timothy Tobery,‡ Diana R. Wetmore, James D. Lear,§ Ara T. Nahapetian, Jodi D. Bradley, and William P. Sisk‖

Crystallography and Biophysical Chemistry Group, The Du Pont Merck Pharmaceutical Company, Du Pont Experimental Station, Wilmington, Delaware 19880

Received October 20, 1993; Revised Manuscript Received June 6, 1994®

ABSTRACT: The binding interactions for the three primary reactants of the fibroblast growth factor (FGF) system, basic FGF (bFGF), an FGF receptor, FGFR1, and the cofactor heparin/heparan sulfate (HS), were explored by isothermal titrating calorimetry, ultracentrifugation, and molecular modeling. The binding reactions were first dissected into three binary reactions: (1) FGFR1 + bFGF ↔ FGFR1/bFGF, K_1 = 41 (±12) nM; (2) FGFR1 + HS ↔ FGFR1/HS, K_2 = 104 (±17) μM; and (3) bFGF + HS ↔ bFGF/HS, K_3 = 470 (±20) nM, where HS = low MW heparin, ~3 kDa. The first, binding of bFGF to FGFR1 in the absence of HS, was found to be a simple binary binding reaction that is enthalpy dominated and characterized by a single equilibrium constant, K_1. The conditional reactions of bFGF and FGFR1 in the presence of heparin were then examined under conditions that saturate only the bFGF heparin site (1.5 equiv of HS/bFGF) or saturate the HS binding sites of both bFGF and FGFR1 (1.0 mM HS). Both 3- and 5-kDa low MW heparins increased the affinity for FGFR1 binding to bFGF by ~10-fold (K_d = 4.9 ± 2.0 nM), relative to the reaction with no HS. In addition, HS, at a minimum of 1.5 equiv/bFGF, induced a second FGFR1 molecule to bind to another lower affinity secondary site on bFGF (K_4 = 1.9 ± 0.7 μM) in an entropy-dominated reaction to yield a quaternary complex containing two FGFR1, one bFGF, and at least one HS. Molecular weight estimates by analytical ultracentrifugation of such fully bound complexes were consistent with this proposed composition. To understand these binding reactions in terms of structural components of FGFR1, a three-dimensional model of FGFR1 was constructed using segment match modeling. Electrostatic potential calculations confirmed that an elongated cluster, ~15 × 35 Å, of nine cationic residues focused positive potential ($+2k_BT$) to the solvent-exposed β-sheet A, B, E, C′ surface of the D(II) domain model, strongly implicating this locus as the HS binding region of FGFR1. Structural models for HS binding to FGFR1, and HS binding to bFGF, were built individually and then assembled to juxtapose adjacent binding sites for receptor and HS on bFGF, against matching proposed growth factor and HS binding sites on FGFR1. The calorimetric binding results and the molecular modeling exercises suggest that bFGF and HS participate in a concerted bridge mechanism for the dimerization of FGFR1 *in vitro* and presumably for mitogenic signal transduction *in vivo*. The thermodynamic driving force for receptor dimerization can be explained in terms of allosteric multivalent binding reactions that allow for the cooperative energetic coupling of heparin binding reactions on FGFR1 and bFGF, reactions 2 and 3, with growth factor/receptor binding events, reactions 1 and 4. Finally, the observation that pentosan polysulfate binds to FGFR1 with a 10-fold higher affinity than HS [K_d = 10.9 (±3.5) μM] may provide an opportunity to reexamine the mechanism of action of this sulfated oligosaccharide and other related inhibitors of angiogenesis currently under investigation for the treatment of breast cancer and AIDS-related Kaposi sarcoma.

There are currently known to be at least nine members of the fibroblast growth factor (FGF)[1] family including acidic FGF (aFGF or FGF-1), basic FGF (bFGF or FGF-2) (Gospodarowicz et al., 1986), keratinocyte growth factor (KGF or FGF-7) (Finch et al., 1989), and the oncogene products *int-2* or FGF-3 (Moore et al., 1986), *hst*/Kaposi-FGF (K-FGF or FGF-4) (Delli Bovi et al., 1988; Taira et al., 1987), FGF-5 (Zhan et al., 1988), and FGF-6 (Marics et al., 1989). All of these proteins bind heparin and share 30–55% identity at the primary amino acid sequence level (Dionne et al., 1990). Various members of the FGF family have been shown to exhibit potent mitogenic activity toward cells of mesenchymal, neuronal, and epithelial origin and to display potent angiogenic properties and are thought to play an important role in

* Author to whom correspondence should be addressed at 3-Dimensional Pharmaceuticals Inc., 3700 Market St., Philadelphia, PA 19104.
‡ Present address: Johns Hopkins University, Baltimore, MD 21218.
§ Present address: University of Pennsylvania, Philadelphia, PA 19104.
‖ Present address: Ares Advanced Technology, Randolph, MA 02368.
® Abstract published in *Advance ACS Abstracts,* July 15, 1994.

[1] Abbreviations: D(I), D(II), and D(III), three extracellular immunoglobulin-like domains of the FGF receptor, where the roman numerals refer to their position relative to the amino terminus; DTT, dithiothreitol; EDTA, disodium salt of ethylenediaminetetraacetic acid; FGF, fibroblast growth factor, where bFGF and aFGF are basic and acidic FGF, respectively; FGFR1, human *flg* FGF receptor, unless otherwise noted; D(II)–D(III) FGFR1, the two extracellular immunoglobulin-like domain truncated form of this receptor; HBGF, heparin binding growth factor; HS, heparin or heparan sulfate-like oligosaccharides; HSPG, heparan sulfate proteoglycan; Hepes, *N*-(2-hydroxyethyl)piperazine-*N*′-2-ethanesulfonic acid; IgSF, immunoglobulin superfamily; ITC, isothermal titrating calorimetry; k_B = Boltzmann constant; kDa, kilodaltons; NaOAc, sodium acetate; PCR, polymerization chain reaction; PMSF, phenylmethanesulfonyl fluoride; PPS, pentosan polysulfate; RT-PCR, reverse transcriptase polymerization chain reaction; SD, standard deviation; Tris, tris(hydroxymethyl)aminomethane.

0006-2960/94/0433-10229$04.50/0

A

```
  1  MWSWKCLLFW AVLVTATLCT ARPSPTLPEQ DALPSSEDDD DDDDSSSEEK
 51  ETDNTKPNPV APYWTSPEKM EKKLHAVPAA KTVKFKCPSS GTPNPTLRWL
101  KNGKGFKPDH RIGGYKVRYA TWSIIMDSVV PSDKGNYTCI VENEYGSINH
151  TYQLDVVERS PHRPILQAGL PANKTVALGS NVEFMCKVYS DPQPHIQWLK
201  HIEVNGSKIG PDNLPYVQIL KTAGVNTTDK EMEVLHLRNV SFEDAGEYTC
251  LAGNSIGLSH HSAWLTVLEA LEERPAVMT
```

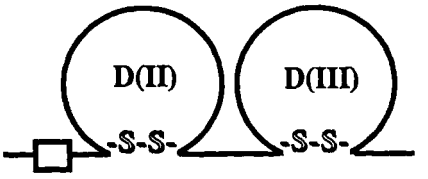

B

```
                (1)
  1  MGTMAAGSIT TLPALPEDGG SGAFPPGHFK DPKRLYCKNG GFFLRIHPDG
 51(39)  RVDGVREKSD PHIKLQLQAE ERGVVSIKGV CANRYLAMKE DGRLLASKCV
101(89)  TDECFFFERL ESNNYNTYRS RKYTSWYVAL KRTGQYKLGS KTGPGQKAIL
151(139)  FLPMSAKS
```

FIGURE 1: (A) Primary amino acid sequences of the extracellular binding domain, D(II)–D(III), of human FGFR1 receptor. The seven potential Asn-linked glycosylation sites (Asn-X-Ser/Thr) are underlined and in bold type. The sequence in italic type refers to the 21 amino acid signal peptide. Amino acids determined by N-terminal sequence analysis (Edman & Begg, 1967) of the purified protein are underlined and are consistent with proper cleavage of the signal sequence *in vivo*. A second minor sequence, NH_2-SXTLXEQDAL–, indicated the presence of a small amount of a truncated receptor protein missing two amino acids at the N-terminus, possibly lost during signal sequence cleavage. The rest of the sequence was translated from the DNA sequence. The boxed sequence refers to the acid box region of FGFR1, an unusual string of acidic residues of unknown function. The conserved cysteines of the IgSF are shown in shadow type. This receptor is similar to the β form isolated from human hepatoma cells but with the site deletion -CTAGCT- (-RM-) previously identified with the γ form of the human liver FGFR1 (Hou et al., 1991). (B) Primary amino acid sequence of human bFGF. The numbers in parentheses correspond to the residues of bFGF numbered according to the scheme of the X-ray crystal structures of Zhang et al. (1991) and Eriksson et al. (1991). Amino acids determined by N-terminal sequence analysis of the purified protein are underlined and were found to be in agreement with that expected from the translated DNA sequence with the initiation Met removed during expression.

embryogenesis (Folkman & Klagsbrun, 1987; Gospodarowicz et al., 1987; Burgess & Maciag, 1989). In adult organisms, the FGFs are thought to play a role in wound healing (Folkman & Klagsbrun, 1987) and in the pathology of tumor growth (Folkman, 1985), rheumatoid arthritis (Melnyk et al., 1990), diabetic retinopathy (Sivalingam et al., 1990), and psoriasis (Sharpe et al., 1989).

The receptors that bind the FGFs also belong to a multigene family. Recently, four closely related genes encoding the FGF receptor subtypes, FGFR1 or *flg* (Lee et al., 1989; Isacchi et al., 1990; Pasquale & Singer, 1989), FGFR2 or *bek* (Dionne et al., 1990; Houssaint et al., 1990), FGFR3 or *cek2* (Pasquale, 1990), and FGFR4 (Partanen et al., 1991; Horlick et al., 1992), have been cloned and characterized. In addition, the mRNAs encoding FGFR1 and FGFR2 are known to undergo several types of alternative splicing (Johnson et al., 1990, 1991). We have cloned a two immunoglobulin-like domain form of the FGFR1 receptor subtype from A159 human endometrial carcinoma cells in culture that is similar to the β form isolated from human hepatoma cells (Hou et al., 1991). The portion of the FGFR1 receptor cDNA that includes the amino-terminal residues comprising the two membrane proximal immunoglobulin superfamily (IgSF) domains of FGFR1 has been cloned and expressed in Sf9 insect cells using a baculovirus expression vector (Figure 1).

To understand the binding interactions of bFGF and its receptor, FGFR1, in molecular detail, a biophysical examination of the energetics of the binding reactions of the FGF system was initiated through isothermal titrating calorimetry (ITC), analytical ultracentrifugation, and molecular modeling. The extent to which the binding energetics for growth factor/receptor interactions are understood and correlated with the available X-ray structures of acidic and basic FGF (Zhang et al., 1991; Eriksson et al., 1991; Zhu et al., 1991; Ago et al., 1991) will largely determine the success of individual efforts to design growth factor antagonists by protein engineering or through structure-based drug design strategies (Kuntz, 1992; Weber et al., 1992, 1994). New antagonists of bFGF/FGFR1 interactions will find applications for the control of angiogenesis and disease states that are neovascularization dependent such as tumor growth and metastasis in addition to several eye diseases (Moses & Langer, 1991; Folkman & Shing, 1992; Harris et al., 1992; Lippman, 1993).

MATERIALS AND METHODS

Chemicals and Reagents. Hepes and dithiothreitol (DTT) were purchased from Research Organics Inc. and used without further purification. Low MW heparin (av 3 kDa) (depolymerized by peroxidolysis of bovine intestinal mucosa), pentosan polysulfate (4 kDa), and PMSF were purchased from Sigma (St. Louis, MO) and used without further purification. Low MW heparin (4800 kDa) which was depolymerized by nitrous acid treatment (lot 011291) was purchased from Calbiochem (San Diego, CA) and is identical to RD Heparin 5000 from Hepar Industries (Franklin, OH). *N*-Glycosidase F was purchased from Boehringer Mannheim (Indianapolis, IN). Prewashed dialysis bags (14-kDa cutoff) were purchased from BRL/Life Technologies Inc. (Gaithersburg, MD). Doubly

distilled and deionized water was used throughout for the preparation of buffers.

Isolation of FGFR1 cDNA. Poly(A^+) mRNA was isolated from cultured A159 human endometrial carcinoma cells using Invitrogen's FastTrack mRNA isolation kit, and cDNA was synthesized from this using the Red Module kit (Invitrogen). Oligonucleotides CTGCATATGTGGAGCTGGAAGTGC (sense) and TTTGGATCCTCAGGTCATCACTGCCG-GCCTCTCTTC (antisense) were used in a PCR reaction to amplify the putative extracellular (binding) domain of the FGFR1 subtype. The reaction was carried out at 94 °C × 1 min, 55 °C × 30 s, and 72 °C × 1 min for 29 cycles, and the resulting 861-bp fragment representing the D(II)–D(III) form of FGFR1 was subcloned into pGEM5 for sequencing. The resulting construct was designated pGEM-FGFR.

Construction of D(II)–D(III) FGFR1 Recombinant Baculovirus. The extracellular domain of FGFR1 was amplified from the initial cDNA construct pGEM-FGFR by PCR. The amplified fragment from pGEM-FGFR encoding amino acids 1–279 (including the putative signal peptide) was gel purified and subsequently ligated into the baculovirus transfer vector pJVP10Z (Vialard et al., 1990). The PCR primers were designed with flanking *Nhe*I sites to facilitate cloning into the *Nhe*I site of the transfer vector. In addition, the 3′ antisense primer contained a translation termination codon (TAA) directly after amino acid residue 279. The resulting transfer vector was designated pJVP-FGFR. Sf9 cells were cotransfected with wild-type AcMNPV viral DNA and the recombinant transfer vector pJVP-FGFR using lipofectin according to the manufacturer's specifications (Life Technologies-Gibco). Lac^+ recombinant baculoviruses were visually screened and plaque purified as described (Vialard et al., 1990; Summers & Smith, 1987). The resulting recombinant baculovirus was designated AcFGFR.

Expression of D(II)–D(III) FGFR1. Sf9 insect cells were infected with the recombinant baculovirus AcFGFR at an MOI of ~5. The cells were grown in Grace's supplemented insect cell media containing 3% calf serum to a density of $\sim 10^9$ cells using a CelliGen bioreactor. After ~72 h the cells were removed by centrifugation (6000*g* for 20 min), and the culture supernatant containing the soluble form of the FGFR1 was stored at −20 °C.

Cloning, Expression, and Purification of bFGF. Poly(A^+) mRNA was isolated from Fogarty's glioma cells and subjected to RT-PCR (Sambrook et al., 1989). The resulting amplified DNA included the coding region from the ATG start codon through the stop codon. The resulting cDNA was cloned and expressed in *Escherichia coli* as described by Squires et al. (1988) and purified using heparin–Sepharose (Shing et al., 1984; Lobb & Fett, 1984; Gospodarowicz et al., 1984) in the presence of 20 mM DTT. Amino-terminal analysis of the purified bFGF indicated the expected sequence and that the initiating Met had been removed by the *E. coli* (Figure 1).

Isothermal Titrating Calorimetry. Samples of purified bFGF and the extracellular D(II)–D(III) FGFR1 were prepared for calorimetry experiments by first concentrating the purified proteins to 20–500 μM using a Centriprep (Amicon, Beverly, MA) centrifugal micro-ultrafiltration device (YM10 membrane; 10-kDa cutoff). The two proteins were placed in separate dialysis bags and then dialyzed against 2 × 1 L of the same buffer solution. In most cases, DTT was present at 1.0 mM to keep the surface cysteines of bFGF reduced during the course of the calorimetry experiments. After dialysis the protein solutions were filtered (0.2 μm) and analyzed by UV–vis absorption spectroscopy to determine the protein concentration (see below).

A MicroCal omega titrating microcalorimeter (MicroCal Inc., Northampton, MA) interfaced with an IBM (386) computer was used to measure the incremental reaction heats for the titration of the primary reactants: bFGF, FGFR1, and low MW heparin. The instrument design and experimental application have been described elsewhere (Wiseman et al., 1989; Brandts et al., 1990: Connelly et al., 1990; Lin et al., 1991). Concentrated D(II)–D(III) FGFR1 or bFGF solutions (20–400 μM) were equilibrated in the reaction cell at 26 °C with stirring (400 rpm) until the baseline noise was 0.005 μcal/s or lower. The solution was then titrated by addition of 20 × 14- or 30 × 9.3-μL aliquots of bFGF, receptor, or HS solutions at 7-min intervals. Measurements were corrected for heats of dilution of ligand into buffer.

The experimental observable measured by the calorimeter is the difference in heat, $\Delta Q_{(i)}$, between the i and $i-1$ injections: $\Delta Q_{(i)} = Q_{(i)} - Q_{(i-1)}$. This reaction heat observed for each ith step for a simple association reaction, $M + X \Leftrightarrow MX$, can be expressed as $\Delta Q_{(i)} = Q_{(i)} - Q_{(i-1)} = \Delta H\,[MX_{(i)} - MX_{(i-1)}]$, where M is the macromolecule in the calorimetric cell, X is the ligand in the syringe, MX is the product,[2] $MX_{(i)}$ is the amount of product present at each step, i, and ΔH is the molar enthalpy of binding. The $[MX_{(i)}]$ will be a function of the $[X]_{total}$, in the cell at step i, the $[M]_{total}$, and the association constant, K_a. A mathematical model that relates the change in the reaction heat with changes in the $[X]_{total}$, $\Delta Q_{(i)}/\Delta[X]_{total}$, to the parameters ΔH, $[M]_{total}$, and n (stoichiometry) and the association constant, K_a, was previously described (Wiseman et al., 1989; Connelly et al., 1990). This model was used to simulate the binding isotherms, and an iterative nonlinear least squares fitting program, ORIGIN (MicroCal), was used to fit the simulated binding isotherms to the experimental $\Delta Q_{(i)}$ by floating n, K_a, and ΔH as fitting parameters in a standard Marquardt fashion for the minimization of the sum of the squared residuals (Wiseman et al., 1989).

A mathematical model for two independent sets of sites and the methods used for the curve fitting were also previously described by Lin et al. (1991). Briefly, the heat content, Q, of the solution within the calorimetric cell of volume V_0 can be described as $Q = [M]_{total}V_0(n_1\theta_1\Delta H_1 + n_2\theta_2\Delta H_2)$, where θ_1 and θ_2 are the fractional saturation quotients, $[MX]/[M]_{total}$ for the two independent binding sites, and are related to the association constants in the following way: $K_1 = \theta_1/(1-\theta_1)[X]$ and $K_2 = \theta_2/(1-\theta_2)[X]$. It is possible to simulate the binding isotherms as described above by making initial guesses for the six fitting parameters, n_1, K_1, ΔH_1, n_2, K_2, and ΔH_2, and calculating $\Delta Q_{(i)calc}$ for comparison with the experimentally observed values, $\Delta Q_{(i)}$, for each ith step, where $\Delta Q_{(i)} = Q_{(i)} - Q_{(i-1)}$. The nonlinear least squares curve fitting was then iterated by allowing the fitting parameters to "float" while utilizing Marquardt methods for the minimization of the sum of the squared residuals (Lin et al., 1991).

Sedimentation Equilibrium Studies. Equilibrium sedimentation of the D(II)–D(III) FGFR1/bFGF complex, in the presence of 1.0 mM low MW heparin, was examined using a Beckman XLA analytical ultracentrifuge. Concentrated solutions of FGFR1 and bFGF were dialyzed separately against 50 mM Hepes, 0.1 M NaCl, and 1.0 mM DTT, as described above for the ITC experiments. Samples were prepared by mixing the reactants in specific mole fractions in the presence of 1.0 mM low MW heparin (~3 kDa). Samples

[2] The convention for titrating calorimetry (Wiseman et al., 1989; Lin et al., 1991; Connelly et al., 1990) is to call whichever reactant in the calorimetric cell the macromolecule, M, and whichever reactant in the syringe the ligand, X.

of 110 μL were loaded along with 10 μL of FC-310 fluorocarbon oil into the standard carbon-filled Epon resin, six channel centerpieces with fused silica windows. Buffer solutions alone were loaded into the corresponding reference compartments. Centrifugation at each noted speed was carried out for at least 20 h (20 °C), a time sufficient to attain equilibrium. Data were analyzed using procedures for nonlinear least squares curve fitting of analytical ultracentrifuge data that we modified from Brooks et al. (1994) to use the Marquart–Levenberg algorithm internal to IgorPro (Wavemetrics, Lake Oswego, OR). Single ideal species curve fits were used to obtain values for the "buoyant" molecular weights, defined as $M_b = M_w(1 - \nu\rho)$, where M_b = buoyant molecular weight, M_w = gram-atomic molecular weight, ν = sedimenting species partial specific volume, and ρ = solvent density in the same units as ν. These values do not depend on assumptions of protein-specific volume (ν), and since exact ν's are not known for the various species, it is convenient to define all molecular weights in this fashion. Conversion of M_b to M_w can be done using estimates of the partial specific volume and solvent density together using the above equation.

Curve-fitting functions were defined to allow simultaneous, weighted least squares fitting of different data sets with buoyant molecular weight (M_b) and baseline absorbance as global parameters. To reduce the number of fitting parameters, baseline absorbance for each cell compartment was determined experimentally by a final centrifugation at 48 000 rpm to deplete protein from the meniscus regions. In concordance with usual practice, data and curve fits were analyzed as optical density–radial distance curves where the fitting function was constrained to intersect the data within the data domain.

Molecular Modeling. Modeling of D(II)–D(III) FGFR1 was performed using the segment match modeling program, SEGMOD, described by Levitt (1992). This software uses a database of highly refined known X-ray structures, such as the IgSF, to build unknown target structures, such as D(II)–D(III) FGFR1, from primary sequence homology. This program matched the D(II) FGFR1 sequence with the coordinates of the C_H2 domain of the Ig Fc fragment (Deisenhofer, 1981). Similarly, the D(III) FGFR1 sequence was matched with the coordinates of the V_H domain of the HYHEL-5 Fab structure of Sheriff et al. (1987). The molecular mechanics program ENCAD (Levitt, 1983) was used for energy minimization of the structures constructed with SEGMOD. The inter-β-sheet disulfide bonds of each domain were formed from the free cysteines using INSIGHTII software (Biosym Corp., San Diego, CA) followed by further energy minimization using the conjugate gradient (2000 steps) subroutine within DISCOVER (v.6.8) and the Consistent valence force field (CVFF) atom potentials within INSIGHTII (v.2.1.1). The simulations were performed on a Silicon Graphics ESX480 workstation. A more comprehensive description of these molecular modeling exercises is in preparation (Pantoliano et al., unpublished results).

RESULTS

Affinity Chromatographic Purification of D(II)–D(III) FGFR1. The strategy employed for the purification of D(II)–D(III) FGFR1 was to first bind 2.0 μmol of bFGF (35 mg) to heparin–Sepharose (Hi-Trap 5-mL column, Pharmacia) under conditions where it is known to bind to this matrix, i.e., 50 mM Hepes, pH 7.5, 0.50 M NaCl, and 20 mM DTT. After the column was washed with the same buffer (no DTT), the resulting bFGF/heparin–Sepharose affinity matrix was equilibrated with the baculovirus-infected insect cell culture media

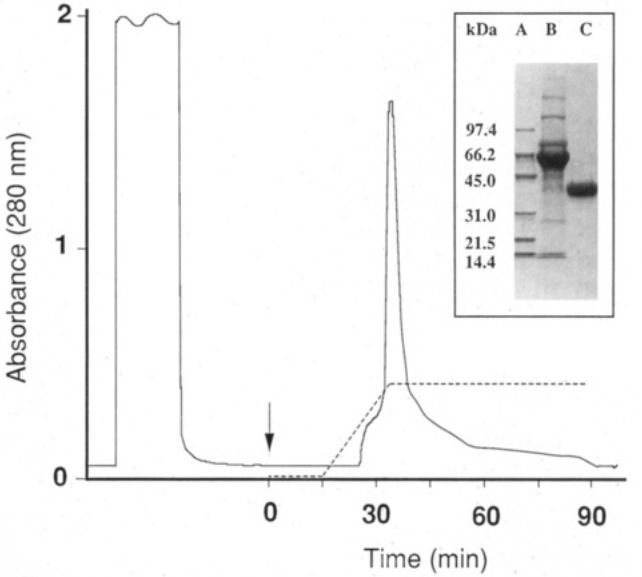

FIGURE 2: Affinity chromatography of D(II)–D(III) FGFR1 using bFGF/heparin–sepharose. Culture media containing secreted receptor was equilibrated with loading buffer (50 mM Hepes, 0.5 M NaCl, pH 7.4) and applied to a 1.5 × 2.5 cm column of bFGF/heparin–sepharose (1.0 mL/min) similarly equilibrated. The column was washed with loading buffer until the absorbance returned to baseline (2–4 h), followed (at arrow) by 6 column volumes of elution buffer A (20 mM NaOAc, pH 5.0, 0.1 M NaCl). A linear gradient of elution buffer B (20 mM NaOAc, pH 5.0, 3.0 M NaCl) was used to develop the profile. The gradient was held at the point where the absorbance peaked (21.0% buffer B or 0.71 M NaCl) until the UV absorbance returned to baseline. Elution was run at 2.0 mL/min at ambient temperature (23 °C). All of these steps were accomplished using a Pharmacia FPLC system. Fractions eluted between 32 and 80 min were pooled, dialyzed against 50 mM Hepes, pH 7.4, and analyzed by SDS–PAGE as shown in the inset. (Inset) SDS–PAGE analysis. The procedure is essentially that of Laemmli (1970) employing prepoured polyacrylamide gradient gels (8–16%) purchased from Novex (Encinitas, CA). Lanes: A, MW standard (kDa) (Bio-Rad low MW markers); B, concentrated baculovirus culture media before being loaded onto the affinity column (major impurity is serum albumin); C, affinity-purified D(II)–D(III) FGFR1 eluted with the pH 5.0 salt gradient. Each lane was loaded with ~20 μg of protein.

containing the secreted D(II)–D(III) FGFR1, washed with starting buffer (no DTT), and selectively eluted at pH 5.0, as described in the legend for Figure 2. The selective elution takes advantage of the reported observation that low pH reduces affinity of bFGF to high-affinity receptors (Moscatelli, 1987) and our observation that bFGF will not elute from heparin–Sepharose at pH 5.0 until [NaCl] ≥ 1.0 M, thereby ensuring that the bFGF remains bound under conditions that elute D(II)–D(III) FGFR1. Control experiments conducted at pH 7.5 and 0.50 M NaCl, but in the absence of bFGF, show that the D(II)–D(III) FGFR1 does not bind to heparin–Sepharose under these conditions.[3]

Preparation of the baculovirus culture media for affinity chromatography was accomplished by simply adjusting the pH of the culture media to 7.5 and [NaCl] to 0.50 M by slow addition of solid Tris base and NaCl, respectively, and loading the resulting solution.[4] Recoveries were ~15 mg of D(II)–

[3] However, when solutions of D(II)–D(III) FGFR1 were equilibrated with heparin–Sepharose (no bFGF) under conditions where the ionic strength was lower (0.1 M NaCl), the binding of D(II)–D(III) FGFR1 was observed, in spite of a p*I* ~5.2 for this protein. Elution of receptor bound to heparin–Sepharose (no bFGF) could be effected by increasing the salt concentration to 0.50 M NaCl. This was an early indication that FGFR1 by itself binds heparin and is consistent with a relatively weak heparin binding site on D(II)–D(III) FGFR1 (see text).

[4] PMSF was present at 0.3 mM in all solutions prior to affinity purification.

D(III) FGFR1/L of culture media with an ~100-fold purification, as judged from A_{280} measurements that employed the ϵ_{280} for this protein (see below). The affinity-purified receptor was estimated to be 93–99% pure, as determined by the observed stoichiometry of the bFGF + FGFR1 ⇔ bFGF/FGFR1 binding reaction (see below) and from the SDS–PAGE analysis (Figure 2).

The affinity chromatographic method of Figure 2 exploits the specific growth factor/receptor binding interactions unique to this protein and has advantages over lectin/carbohydrate methods (Kiefer et al., 1991). For example, this scheme can be used to purify deglycosylated forms of this protein prepared by enzymatic deglycosylation (see below) or through expression in *E. coli* and refolding using procedures for reversible folding of other members of IgSF (Pantoliano et al., 1991). In this latter application the scheme of Figure 2 has the important ability to discriminate between active and inactive forms of FGFR1. Furthermore, this strategy may be adapted for the purification of FGFR2, FGFR3, FGFR4, KGFR, etc. and their variant alternatively spliced forms (Johnson et al., 1990, 1991; Miki et al., 1992; Jaye et al., 1992) with minor modifications.[5] This affinity chromatography strategy may also be useful for other receptors that bind heparin binding proteins that are outside the FGF family.[6]

Extinction Coefficient for D(II)–D(III) FGFR1. The extinction coefficient at 280 nm was determined for this protein by first measuring the UV absorption spectrum of purified (filtered) protein solutions and then submitting the samples to acid hydrolysis and amino acid composition analysis. The [protein] was then calculated on the basis of the observed quantities of Asx, Glx, Ala, Pro, Leu, and Lys released upon acid hydrolysis and their known frequency in the primary sequence translated from the gene. The molar extinction coefficient for D(II)–D(III) FGFR1 calculated in this way was found to be ϵ_{280} = 46 732 (±279) M^{-1} cm^{-1} for five determinations. It was also possible to calculate an $E^{0.1\%}$ = 1.17 (±0.01) after measuring the FGFR1 molecular weight. A MW of ~40 000 was determined by D(II)–D(III) FGFR1 migration upon SDS–PAGE analysis (see Figure 2), which was found to be in agreement with a MW = 39 900 (±3000) determined from a size-exclusion HPLC column (G3000 PWXL) under native conditions. The ϵ_{280} was also estimated by the frequency of Trp and Tyr residues in the translated primary amino acid sequence of the gene by employing the individual molar extinction coefficients (ϵ = 1413 M^{-1} cm^{-1} for Tyr; ϵ = 6310 M^{-1} cm^{-1} for Trp) near 280 nm (*Handbook of Chemistry and Physics*, 55th ed.). The calculated ϵ_{280} = 44 267 M^{-1} cm^{-1} (5 Trp and 9 Tyr) was in close agreement with that measured by amino acid composition.

Extinction Coefficient for bFGF. A similar analysis for bFGF revealed ϵ_{280} = 16 766 (±239) M^{-1} cm^{-1} ($E^{0.1\%}$ = 0.96 ± 0.02 using MW = 17 400) for six determinations of bFGF amino acid composition. The MW for bFGF was based on the translated primary amino acid sequence for its gene. The calculated ϵ_{280} = 16 201 M^{-1} cm^{-1} (1 Trp and 7 Tyr) was also in close agreement with that determined by amino acid composition.

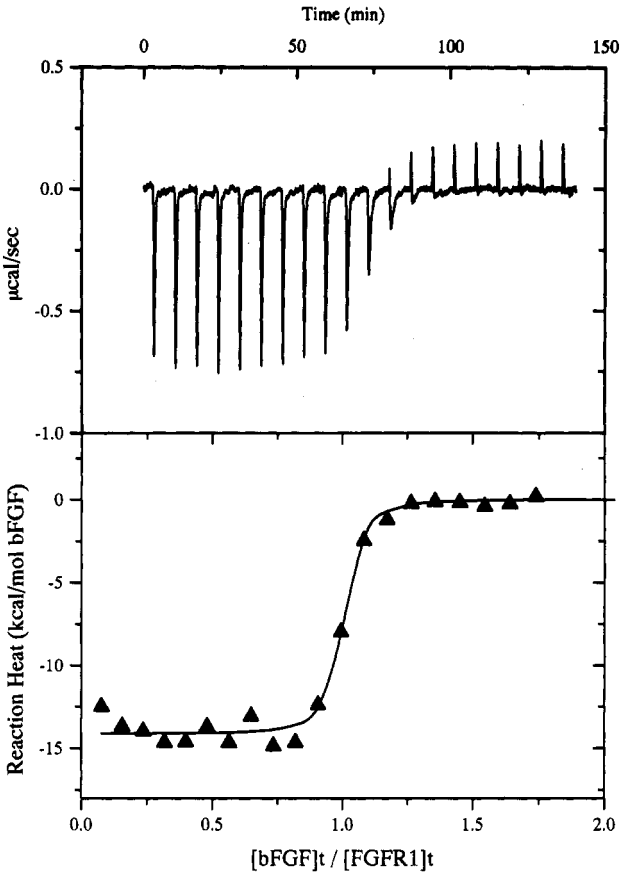

FIGURE 3: Binding isotherm for the bFGF titration of D(II)–D(III) FGFR1 in the absence of heparin at 26 °C and pH 7.5. (Top) An 18.2 µM solution of D(II)–D(III) FGFR1 (M) was equilibrated in the calorimetric cell and titrated with 20 14-µL injections (14 µL delivered over a 12-s duration) of 110 µM bFGF (X) by employing an injection schedule that separated the additions by 7 min. The rate of this reaction was sufficiently fast under these conditions (k_{on} = 2.5 × 10^8 M^{-1} min^{-1}; Nugent & Edelman, 1992) that this injection schedule allowed complete equilibration between additions. (Bottom) The area under each injection signal, $\Delta Q_{(i)}$, was integrated and plotted in the bottom panel as a function of the mole ratio of the reactants, after subtraction of the blank. The solid line represents a nonlinear least squares fit of the reaction heat for each injection ($\Delta Q_{(i)}$) with the assumption of a single binding site comprised of the three fitting parameters, n, K_a, and ΔH, which were all allowed to "float" during computer iterations (see Materials and Methods). This experiment was carried out a number of times under various conditions, and the results are summarized in Table 1.

N-Terminal Sequence Analysis of D(II)–D(III) FGFR1 and bFGF. Results for N-terminal sequence analysis for purified samples of FGFR1 and bFGF appear in Figure 1 and are consistent with the sequence expected from the cDNA expression constructs.

Deglycosylation of D(II)–D(III) FGFR1. The extent of glycosylation of the receptor was examined by treating the purified protein with *N*-glycosidase F[7] (Tarentino et al., 1985) for ~17 h at 23 °C, followed by repurification of the D(II)–D(III) FGFR1 by affinity chromatography. The deglycosylated receptor could be bound and eluted from the affinity

[5] The best growth factor to use as the heparin-bound ligand will depend on the known differences in binding selectivity. For example, KGF or aFGF would be preferable to bFGF for the purification of KGFR because of the poor binding of bFGF to KGFR (Miki et al., 1992). Other modifications may be needed to accommodate the differences in pH and salt dependence of the heparin/HBGF/FGFR interactions likely to be encountered.

[6] The HBGF family now includes platelet-derived growth factor (PDGF), vascular endothelial cell growth factor (VEGF), heparin binding epidermal growth factor (HB-EGF; Higashiyama et al., 1992), granulocyte macrophage colony stimulating factor (GM-CSF; Roberts et al., 1988), interleukin-3 (Roberts et al., 1988), osteogenin (Luyten et al., 1989; Wozney et al., 1988), hepatocyte growth factor (HGF), Schwannoma-derived growth factor, and pleiotrophin (Klagsbrun & Baird, 1991; Chauhan et al., 1993).

[7] *N*-Glycosidase F cleaves the *N*-glycan linkage of glycoproteins between asparagine and the carbohydrate chain. The enzymatic cleavage reaction was conducted under native and denaturing conditions to examine whether native conditions were sufficient for the effectual removal of the carbohydrate chains. Analysis by SDS–PAGE confirmed that heat denaturation and detergents gave the same extent of carbohydrate removal.

Table 1

(A) Binding Parameters for Titration of bFGF into D(II)–D(III) FGFR1 Solutions[a]

ligand	[DTT] (mM)	[FGFR1] in cell (μM)	K_d[b] (nM)	n	$\Delta G°$ (kcal/mol)	ΔH (kcal/mol)	$T\Delta S$ (kcal/mol)
bFGF	0.0	4.1	27.0 (±7.3)	0.98 (±0.02)	−10.4	−12.2 (±0.3)	−1.8
bFGF	0.0	4.1	55.6 (±21.6)	1.01 (±0.03)	−9.9	−12.0 (±0.4)	−2.1
bFGF	1.0	18.2	43.5 (±17.0)	0.93 (±0.01)	−10.1	−10.7 (±0.2)	−0.6
bFGF	1.0	18.2	52.6 (±55.4)	0.95 (±0.03)	−10.0	−10.7 (±0.6)	−0.7
bFGF	1.0	20.1	32.3 (±20.8)	0.84 (±0.02)	−10.3	−10.5 (±0.3)	−0.2
bFGF	1.0	20.1	50.0 (±25.0)	0.82 (±0.01)	−10.0	−11.0 (±0.3)	−1.0
bFGF	1.0	32.2	26.3 (±20.8)	0.98 (±0.01)	−10.4	−11.1 (±0.3)	−0.7
			41.0 (±12.4)	**0.93 (±0.07)**	**−10.2 (±0.2)**	**−11.2 (±0.7)**	**−1.0 (±0.7)**

(B) Binding Parameters for Titration of D(II)–D(III) FGFR1 into bFGF Solutions[c]

ligand	[bFGF] in cell (μM)	K_d[b] (nM)	n	$\Delta G°$ (kcal/mol)	ΔH (kcal/mol)	$T\Delta S$ (kcal/mol)
FGFR1	18.9	47.6 (±20.4)	0.93 (±0.01)	−10.0	−15.0 (±0.4)	−5.0
FGFR1	18.9	50.0 (±17.5)	0.90 (±0.01)	−10.0	−13.8 (±0.3)	−3.8
		48.8 (±2.0)	**0.92 (±0.02)**	**−10.0 (±0.02)**	**−14.4 (±0.8)**	**−4.4 (±0.8)**

[a] All experiments were performed at 26 °C in 50 mM Hepes, pH 7.5, and 100 mM NaCl. The ligand, bFGF, was titrated into the reaction cell which contained D(II)–D(III) FGFR1 solutions at the concentrations shown. The data were analyzed with the assumption of one set of sites. [b] The numbers within parentheses are the uncertainty for the fitting parameters found for individual experiments. The numbers in parentheses that appear next to the mean value (in bold type) represent ±1 SD for the group of individual experiments used in the calculation of the mean (seven experiments). Calculations of thermodynamic state functions were determined from $\Delta G° = -RT \ln K_a$, $\Delta G° = \Delta H - T\Delta S$, and $K_a = 1/K_d$; 1.0 kcal/mol = 4.184 kJ/mol. [c] The ligand, D(II)–D(III) FGFR1, was titrated into the reaction cell which contained bFGF solutions at the concentrations shown.

matrix in the same way as the untreated protein. SDS–PAGE analysis revealed that the diffuse doublet band at ~40 000 for the untreated FGFR1 was changed to a sharp single band at ~33 000. The lower MW is consistent with the MW = 28 700 expected from the amino acid sequence (Figure 1). Thus, 20 to 40% of the MW of baculovirus-derived D(II)–D(III) FGFR1 can be attributed to Asn-linked glycosylation, accordant with the seven potential Asn-linked glycosylation sites (Figure 1A).

The similar characteristics of the glycosylated and deglycosylated forms of FGFR1 for binding to and elution from the bFGF/heparin–Sepharose affinity matrix suggest that the carbohydrate moieties do not play a significant role in the binding interactions to the growth factor. This was also confirmed through competition assays of the glycosylated and deglycosylated forms of FGFR1 that employed BHK cells or rat lung membranes where IC_{50} values were found to be the same within experimental error. These observations are consistent with those of Kiefer et al. (1991) and Bergonzoni et al. (1992) for the three domain version, D(I)–D(II)–D(III), of FGFR1.

Isothermal Titrating Calorimetry. The binding reactions of the primary reactants, D(II)–D(III) FGFR1, bFGF, and low MW heparin, were investigated by isothermal titrating calorimetry (ITC). The three binary binding reactions for these reactants were first investigated individually and then conditionally in the presence of low MW heparin.

Binary Binding Reactions of bFGF, D(II)–D(III) FGFR1, and HS. (A) bFGF Titration of D(II)–D(III) FGFR1 in the Absence of HS. In the absence of HS, bFGF bound to D(II)–D(III) FGFR1 in an exothermic manner with a $K_d = 41 \pm 12$ nM and a stoichiometry of nearly 1:1, as shown in Figure 3 and Table 1. This binary binding reaction was studied under a variety of conditions which included (a) reversing the order of addition of reactants, (b) altering the buffer present during the reaction (Hepes–NaOH, or Tris-HCl, at 50 mM and pH 7.5), (c) varying the concentration of the D(II)–D(III) FGFR1 while titrating with bFGF, and (d) adjusting the [DTT] present during the reaction.

The results for the titration experiments performed by addition of bFGF to solutions of D(II)–D(III) FGFR1 in the calorimetric cell at T = 26 °C , pH 7.5 (50 mM Hepes–NaOH), 0.10 M NaCl, and 1.0 mM DTT are presented in Table 1. The titration experiments were performed at different [FGFR1] in the cell (4–32 μM) to examine the molecularity of the reaction. For each experiment the data could be fit to a simple single-site reaction model with the same observed fitting parameters within experimental error. The lack of evidence for a [protein] dependence for this binding reaction suggests that there is no significant change in the aggregation state of either protein in this concentration range or upon binding under the conditions employed for these experiments. The results obtained in 0 and 1.0 mM DTT are not significantly different (Table 1), suggesting that intermolecular disulfide bond formation for bFGF does not occur under these conditions.

(B) D(II)–D(III) FGFR1 Titration of bFGF in the Absence of HS. The reversibility of the order of addition of binding reactants was explored by carrying out the titration in the reverse direction where the reaction progressed from low to high receptor:FGF ratios rather than from high to low, as discussed above. The results for those experiments are presented in Table 1 and show that the binding parameters are essentially the same. This degree of reversibility for the order of addition of reactants further supports the 1:1 binary binding mode of growth factor/receptor with K_d = 48.8 nM, in the absence of HS.

(C) Effect of Buffers on the bFGF Titration of D(II)–D(III) FGFR1 in the Absence of HS. In order to test the effect of buffers on the binary reaction of bFGF and FGFR1 and to examine the role of protons in this reaction, the ITC experiments were also performed using Tris-HCl under the same conditions (pH 7.5, 50 mM, and 0.10 M NaCl) as described above for Hepes–NaOH. The results for these experiments are summarized in Table 2 and show that the binding parameters are slightly different ($K_d = 20 \pm 12$ nM in Tris-HCl buffer compared with $K_d = 41 \pm 12$ nM) but not necessarily significant given the observed error bars. Moreover, there is a small decrease in the observed $\Delta H°_{bind}$ that correlates with the enthalpy of ionization, $\Delta H°_{ion}$, of the two buffers tested: +3.9 and +11.3 kcal/mol for Hepes and Tris, respectively (Grimes, 1985). If protons participate in the binding reaction, then $\Delta H°_{ion}$ of the buffer would be superimposed on the enthalpy of bFGF binding to FGFR1 in

Table 2: Effect of Tris-HCl Buffer on the Titration of bFGF into D(II)–D(III) FGFR1 Solutions[a]

ligand	[FGFR1] in cell (μM)	K_d[b] (nM)	n	$\Delta G°$ (kcal/mol)	ΔH (kcal/mol)	$T\Delta S$ (kcal/mol)
bFGF	22.9	15.7 (±7.4)	1.04 (±0.01)	−10.7	−13.0 (±0.4)	−2.3
bFGF	22.9	32.3 (±10.4)	0.98 (±0.01)	−10.3	−13.9 (±0.2)	−3.6
		20.0 (±11.7)	**1.01 (±0.04)**	**−10.5 (±0.3)**	**−13.5 (±0.6)**	**−3.0 (±0.9)**

[a] These experiments were performed at 26 °C in 50 mM Tris-HCl bluffer, pH 7.5, 100 mM NaCl, and 1.0 mM DTT. The data were analyzed as described in the text. [b] See footnote *b* of Table 1 for a description of the binding parameters.

the data of Tables 1 and 2. This can be analyzed by plotting the $\Delta H°_{ion}$ vs $\Delta H°_{bind}$ due to the linear relationship $\Delta H°_{bind} = \Delta H°_{react} + N_H(\Delta H°_{ion})$, where $\Delta H°_{bind}$ is the observed enthalpy under any given condition, $\Delta H°_{react}$ (y intercept) is the enthalpy, independent of buffer and pH effects, and N_H (slope) is the number of protons released during the reaction which consequently bind to the buffer (Murphy et al., 1993). Plotting the data obtained in Hepes and Tris-HCl buffers in this way suggested that ~0.30 protons are released upon binding of bFGF to D(II)–D(III) FGFR1 at pH 7.5 and that the proton-independent enthalpy can be extrapolated to $\Delta H°_{react} = -10.0$ kcal/mol. Additional experiments in other buffers are needed to confirm this result.

(D) Heparin and Pentosan Polysulfate Binding to D(II)–D(III) FGFR1 in the Absence of bFGF. The reaction heat titration data and the resultant binding isotherm for the titration of D(II)–D(III) FGFR1 with low MW heparin (3 kDa) are shown in Figure 4. The rate of this reaction was found to be faster than the reaction of bFGF with FGFR1 in Figure 3 ($k_{on} = 2.5 \times 10^8$ M^{-1} min^{-1}; Nugent & Edelman, 1992), so that the equal volumes of injected HS solution (14 μL delivered over a 12-s duration) spaced at 7-min intervals were sufficient to allow complete equilibration between injections. The experiment was conducted three times to yield K_d = 104 (±17) μM, n = 1.39 (±0.06), and ΔH = −5.63 (±0.07) kcal/mol. Similarly, the data for the titration of D(II)–D(III) FGFR1 with low MW heparin (5 kDa), RD Heparin 5000, is shown in Figure 5. In this case the binding parameters were found to be K_d = 85 (±7) μM, n = 1.17 (±0.02), and ΔH = −7.48 (±0.2) kcal/mol.

The titration of D(II)–D(III) FGFR1 with pentosan polysulfate (PPS) was also examined. This sulfated oligosaccharide was found to bind to D(II)–D(III) FGFR1 with ~10-fold higher binding affinity: K_d = 10.9 (±3.5) μM, n = 0.83 (±0.06), and ΔH = −12.1 (±0.95) kcal/mol (Figure 6). These values represent the mean for two independent experiments.

The titrations of FGFR1 with low MW heparin (3 and 5 kDa) and PPS fit to single binding equilibria with stoichiometries of ~1:1, and the closeness of the computer-generated fits could be judged from the plots of the reaction heats vs aliquot injection values in Figures 4–6. Testing the reversibility of these reactions, where FGFR1 is titrated into HS, was not feasible due to the millimolar concentrations of FGFR1 required. Notwithstanding this inspection of reversibility, these reactions appear to be specific binary binding reactions with thermodynamic parameters that approximate those expected for two homogeneous reactants: saturation binding with ~1:1 stoichiometry over a wide range of fractional saturation, $\theta = [FGFR1/HS]/[FGFR1]_{total}$ = 0.09–0.82, in the two cases of low MW heparin (3 or 5 kDa), and θ = 0.09–0.90, in the case of PPS. The homogeneity of FGFR1 could be judged to be ~93–99% pure from Figure 2 as discussed above. The homogeneity of the HS derivatives, however, should not be assumed due to the commonly observed variation in degree of sulfation and range of MW which are variables related to the synthesis of HS by cells (Gallagher & Turnbull, 1992; Yanagishita & Hascall, 1992) and the

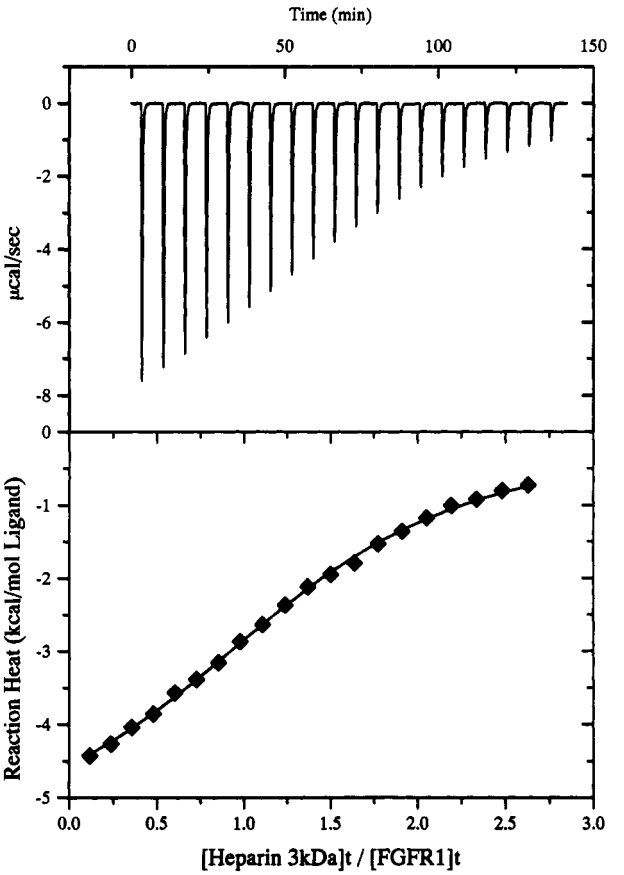

FIGURE 4: Low MW heparin (3 kDa) binding to D(II)–D(III) FGFR1. A 3.56 mM solution of low MW heparin (~3 kDa) was titrated into a 333 μM D(II)–D(III) FGFR1 solution using a 20 × 14-μL injection schedule spaced at 7-min intervals (T = 25.6 °C). The D(II)–D(III) FGFR1 solution had been dialyzed vs 2 × 1 L of 50 mM Hepes and 0.10 M NaCl, and the heparin solution was prepared gravimetrically by dissolving solid low MW heparin in the same buffer. (Top) Raw titration data for D(II)–D(III) FGFR1 showing the 20 individual changes in $Q_{(i)}$ after each injection of heparin. (Bottom) Resultant binding isotherm for low MW heparin titration of D(II)–D(III) FGFR1 after integration of the area under each injection peak and subtraction of the blank. The experimental data were fit in the same manner as described for Figure 3. This experiment was carried out three times, and a summary of the binding parameters are K_d = 104 (±17) μM, n = 1.36 (±0.14), and ΔH = −5.57 kcal/mol.

method of depolymerization by commercial sources. The low MW heparin samples, 3 kDa and RD Heparin 5000 (5 kDa), are from two different commercial sources and were prepared by two different depolymerization methods, peroxidolysis and nitrous acid, respectively. Nevertheless, each was found to bind to FGFR1 with very similar binding parameters (Figures 4 and 5), suggesting that the microheterogeneity of each sample either is too small to detect or does not result in large changes in the binding affinity to FGFR1.[8] One would expect to be able to detect by ITC a subspecies of low MW heparin that

[8] Similar results were observed upon binding of 3- and 5-kDa low MW HS samples to bFGF (Thompson et al., 1994).

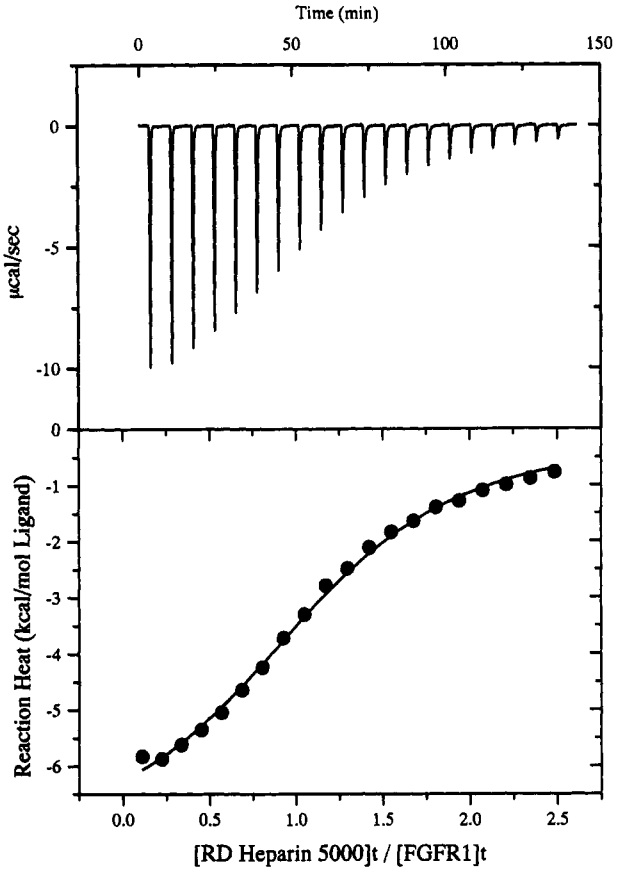

FIGURE 5: Low MW heparin (5 kDa) binding to D(II)–D(III) FGFR1. A 3.46 mM solution of low MW heparin (~5 kDa), RD Heparin 5000, was titrated into a 342 µM D(II)–D(III) FGFR1 solution using a 20 × 14-µL injection schedule spaced at 7-min intervals (T = 25.5 °C). The D(II)–D(III) FGFR1 solution had been dialyzed vs 2 × 1 L of 50 mM Hepes and 0.10 M NaCl, and the heparin solution was prepared gravimetrically by dissolving solid low MW heparin (RD Heparin 5000) in the same buffer. (Top) Raw titration data for the 20 individual changes in $Q_{(i)}$ after each injection of heparin. (Bottom) Binding isotherm for low MW (5 kDa) heparin titration of D(II)–D(III) FGFR1. The experimental data were fit in the same manner as described for Figure 3. This experiment was carried out twice, and a summary of the binding parameters are K_d = 85.3 (±10) µM, n = 1.17 (±0.14), and ΔH = −7.48 kcal/mol.

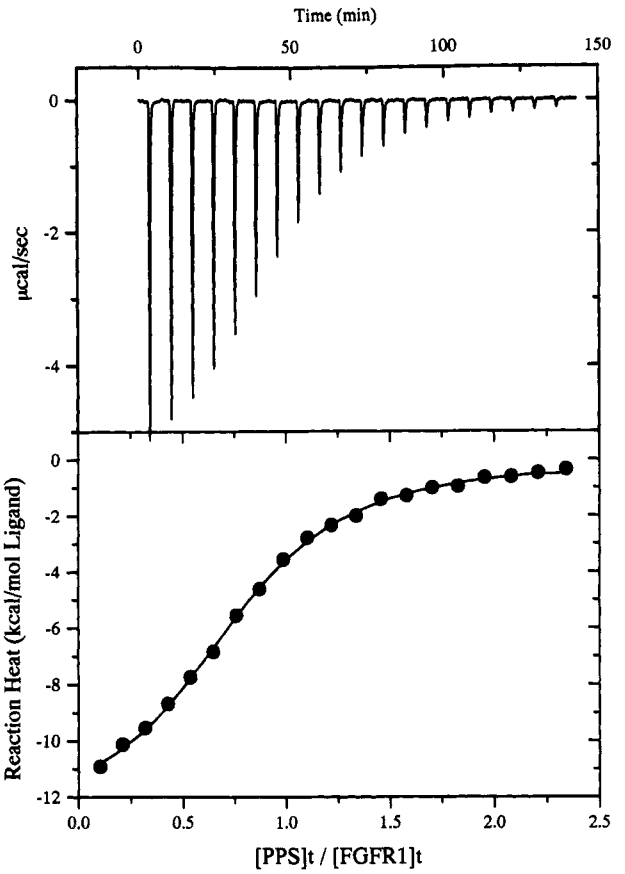

FIGURE 6: Pentosan polysulfate binding to D(II)–D(III) FGFR1. A 1.0 mM solution of PPS (4 kDa) was titrated into a 105 µM D(II)–D(III) FGFR1 solution using a 20 × 14-µL injection schedule spaced at 7-min intervals (T = 25.6 °C). The D(II)–D(III) FGFR1 solution had been dialyzed vs 2 × 1 L of 50 mM Hepes and 0.10 M NaCl, and the PPS solution was prepared gravimetrically by dissolving solid PPS in the same buffer. (Top) Raw titration data for D(II)–D(III) FGFR1 showing the 20 individual changes in $Q_{(i)}$ after each injection of PPS. (Bottom) Resultant binding isotherm for PPS titration of D(II)–D(III) FGFR1 after integration of the area under each injection peak and subtraction of the blank. The experimental data were fit in the same manner as described for Figure 3. This experiment was carried out twice, and a summary of the binding parameters are K_d = 10.9 (±3.5) µM, n = 0.83 (±0.06), and ΔH = −12.1 (±0.95) kcal/mol.

comprised as little as 0.15 mole fraction of the sample but with ≥5-fold increase in binding affinity than the majority of the sample. The absence of bi- or multicomponent binding isotherms, together with the indifference to the method of preparation or commercial source of the two heparin derivatives, suggests that the average binding characteristics of low MW heparin to FGFR1 can be approximated by the single binding equilibria reported in Figures 4 and 5. The results for FGFR1/PPS binding in Figure 6 support this supposition since the ~10-fold increase in binding affinity of this sulfated oligosaccharide permitted a higher degree of fractional saturation at the end of the titration (θ = 0.90), yet retaining good fidelity to a single binding equilibrium throughout the binding isotherm. Confirmation of these results must wait until sufficient quantities of homogeneous low MW HS derivatives (Tyrrell et al., 1993) become more widely available.

Additional support for the single binding equilibria description for HS binding to FGFR1 with modest binding affinity comes from the binding of D(II)–D(III) FGFR1 to heparin–Sepharose when the ionic strength is low (0.1 M NaCl, pH = 7.5). The elution of FGFR1 from heparin–Sepharose could be effected as a single relatively sharp peak by applying a linear salt gradient from 0.1 to 1.0 M NaCl (FGFR1 elutes near 0.37 M NaCl at pH 7.5; data not shown). A collection of many different species of immobilized heparin due to microheterogeneity would be expected to yield a much more complicated elution profile, depending on the number and relative affinities of the individual components.

Conditional Reactions of bFGF and D(II)–D(III) FGFR1 in the Presence of Low MW Heparin. (A) D(II)–D(III) FGFR1 Titrations of bFGF While Saturating the HS Binding Sites of both FGFR1 and bFGF with 1.0 mM Low MW Heparin. In order to examine the binding parameters of bFGF and FGFR1 while saturating the heparin binding site of FGFR1, the ITC experiments of Table 1 were repeated in the presence of 1.0 mM heparin. This concentration of heparin, which is ~10-fold above the observed K_d for heparin/FGFR1 binding (see above), will also ensure that the heparin binding site of bFGF is saturated as well (K_d = 470 ± 20 nM; Thompson et al., 1994). The binding isotherm for the titration of bFGF with D(II)–D(III) FGFR1 under these conditions is shown in Figure 7. The binding reaction can be divided into two parts: (1) the growth factor is in excess for the early additions of receptor, and at this stage of the reaction the data can be fit to one high-affinity binding reaction of K_1 = 5.3 ± 4.5 nM with ~1:1 binding stoichiometry and ΔH = −13.9 ± 0.7 kcal/mol; (2) following addition of 1.0 mol equiv of receptor to bFGF, the data were found to be consistent with a second but weaker binding reaction with K_2 = 1.2 ± 0.4 µM, also of 1:1

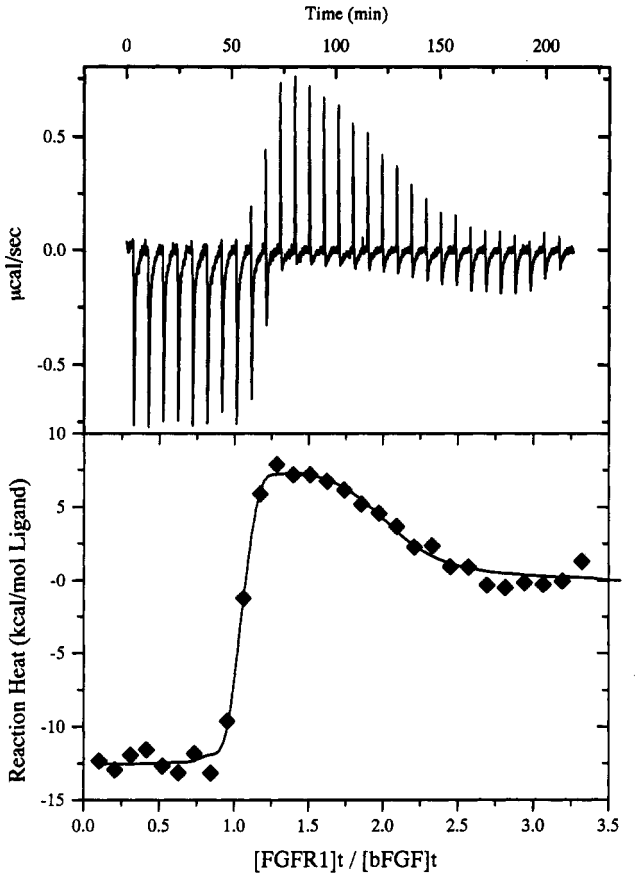

FIGURE 7: D(II)–D(III) FGFR1 titration of bFGF while saturating both receptor and bFGF with 1.0 mM low MW heparin. This experiment was conducted by first dialyzing stock solutions of bFGF and D(II)–D(III) FGFR1 in separate dialysis bags against 50 mM Hepes, pH 7.5, 0.10 M NaCl, and 1.0 mM DTT, at 4 °C (2 × 1 L changes). The bFGF was diluted to 23.5 μM (5.0 mL) and made 1.0 mM in low MW heparin (~3kDa) by adding 135 μL of a 37 mM HS stock solution (prepared in dialysate buffer). (Top) The resulting bFGF/heparin solution was then equilibrated in the calorimetric cell at 25.9 °C and titrated with 30 × 9.3-μL injections of 322 μM D(II)–D(III) FGFR1 (similarly made 1.0 mM in low MW HS) by employing an injection schedule that separated the additions by 7 min. The raw data for this titration are shown in the top panel. Control experiments were conducted by titrating FGFR1 (1.0 mM heparin) into buffer solutions (1.0 mM heparin) with no bFGF present. The raw data for these control injections were similar to the last four or five injections near the end of the sample titration. (Bottom) Resultant binding isotherm for D(II)–D(III) FGFR1 titration of bFGF in the presence of 1.0 mM HS after integration of the area under each injection peak and subtraction of the blank (titration of FGFR1 into buffer, 1.0 mM in HS). The solid line represents a nonlinear least squares fit of the reaction heat for each injection ($\Delta Q_{(i)}$) with the assumption of two independent sites comprised of the six fitting parameters, n_1, K_1, ΔH_1, n_2, K_2, and ΔH_2, which were all allowed to float during computer iterations (see Materials and Methods). The convergent best fit for this experiment was found for n_1 = 0.97 (±0.01), K_1 = 1.3 (±1.0) nM, ΔH_1 = −12.9 (± 0.30) kcal/mol, n_2 = 0.97 (±0.06), K_2 = 0.91 (±0.43) μM, and ΔH_2 = +8.5 (±0.75) kcal/mol. The error estimates (±1.0 SD) in parentheses for the fitting parameters correspond to the nonlinear least squares fit for the experimental data points for this particular experiment. The experiment was repeated three times in Hepes and once in Tris-HCl buffer, and the results are summarized in Table 3.

stoichiometry, and ΔH = +8.3 ± 0.1 kcal/mol. This experiment was repeated three times in Hepes and once in Tris-HCl buffer (50 mM , pH 7.5, 0.1 M NaCl), and the results are summarized in Table 3. Similar results were obtained when 1.0 mM RD Heparin 5000 was substituted for low MW heparin (3 kDa) in this conditional reaction (data not shown).

The results in Tris-HCl buffer are very similar to those in Hepes except that in this case the ΔH values for both receptor/bFGF reactions, ΔH_1 and ΔH_2, are more negative by ~2.4 kcal/mol. This result is similar to that described for the reaction in the absence of HS (Table 2) and is again consistent with the release of ~0.3 proton per receptor binding event at pH 7.5. A proton-independent ΔH extrapolates to $\Delta H°_{react}$ = −12.5 kcal/mol for site 1 and +9.5 kcal/mol for site 2.

The ~10-fold potentiation of binding affinity for K_1 in the presence of low MW heparin brings the affinity of the bFGF/FGFR1 reaction to an approach to the limit of measurement of K_d using ITC (Wiseman et al., 1989). The reaction, as observed in Figure 7, is beginning to approximate an end-point titration since the number of points in the transition region used for estimates of K_d are becoming fewer with each increase of the bFGF/FGFR1 binding affinity. This is reflected in the larger error bars obtained for the nonlinear least squares fits and reduces the ability to distinguish between K_d = 5 and 1 nM. Therefore, the K_1 values reported in Tables 3–5 should be considered apparent K_d's and use the error estimates as an indication of the uncertainty inherent for these measurements.

(B) bFGF Titrations of D(II)–D(III) FGFR1 While Saturating the Heparin Binding Sites of both FGFR1 and bFGF with Low MW Heparin. The reversibility of the FGFR1/bFGF binding reaction was examined by performing the titration in the reverse direction by progressing from high to low receptor:FGF ratios rather than from low to high, as discussed above. A representative binding isotherm for bFGF titration of D(II)–D(III) FGFR1 in the presence of 0.62 mM low MW heparin is shown in Figure 8. This binding isotherm can also be divided into two parts: an early phase that occurs between 0 and ~0.5 equiv of bFGF and a second phase that occurs between $[bFGF]_t/[FGFR1]_t$ = ~0.5 and 1.0. After addition of 1.0 equiv of bFGF the incremental reaction heats return to baseline. This result is also consistent with two binding sites on bFGF for D(II)–D(III) FGFR1 as observed in Figure 7, because in this case the receptor is in excess, and the early additions of growth factor will result in two simultaneous receptor binding reactions on bFGF with a reaction heat of $\Delta H_1 + \Delta H_2$. This analysis anticipates that once sufficient bFGF has been added ($[bFGF]_t/[FGFR1]_t$ = ~0.5) to engage all of the receptor in a 2 to 1 complex; then further additions of bFGF will result in receptor displacement from the lower affinity site in the 2 to 1 complex in favor of binding to the ~250-fold higher affinity binding site on newly added bFGF. The heat change for the second phase of the reaction is $\Delta H_1 - \Delta H_2$, since site 1 has a somewhat higher affinity than site 2. Under these conditions, all of the FGFR1 is in the 1:1 complex when the molar ratio reaches ~1.0, and additional injections of bFGF result in no further reaction heat, i.e., return to baseline.

This reaction was repeated six times using different concentrations of 3-kDa low MW HS (0.64–0.11 mM), and the results were found to be essentially the same in each case, as shown in Table 4. The binding isotherms were resolved into their composite binding site parameters using a two-site fitting strategy to simulate the simultaneous binding events using the data for site 1 and site 2 obtained for the reverse direction of reactant additions (Figure 7) as a starting point for curve fitting. The larger variability for these binding parameters, when compared to the results reported in Tables 1–3, reflects the uncertainty involved in attempting to fit two bFGF/FGFR1 binding reactions that are not sequentially isolated, as they are for the reverse reactions in Figure 7. However, there is a strong agreement between the two collective sets of data since both implicate 2.0 mol equiv of FGFR1 binding per 1.0 mol equiv of bFGF. The first receptor

Table 3: Binding Parameters for Titration of D(II)–D(III) FGFR1 into bFGF Solutions in the Presence of 1.0 mM Low MW Heparin (3 kDa)[a]

	site 1			site 2		
buffer (pH 7.5)	K_1[b] (nM)	n_1	ΔH_1 (kcal/mol)	K_2 (μM)	n_2	ΔH_2 (kcal/mol)
Hepes	2.9 (±0.9)	0.99 (±0.01)	−14.2 (±0.15)	1.8 (±0.44)	1.16 (±0.03)	+8.2 (±0.3)
Hepes	11.5 (±5.3)	0.87 (±0.01)	−14.6 (±0.34)	1.0 (±0.35)	1.07 (±0.04)	+8.3 (±0.6)
Hepes	1.3 (±1.0)	0.97 (±0.01)	−12.9 (±0.30)	0.91 (±0.43)	0.97 (±0.06)	+8.5 (±0.7)
mean	**5.3 (±4.5)**	**0.94 (±0.05)**	**−13.9 (±0.73)**	**1.2 (±0.40)**	**1.07 (±0.08)**	**+8.3 (±0.1)**
Tris	1.5 (±4.6)	1.06 (±0.01)	−16.5 (±0.32)	0.91 (±2.5)	1.34 (±0.29)	+6.1 (±1.0)

[a] All experiments were performed at 26 °C in 50 mM buffers at pH 7.5 and 100 mM NaCl. Low MW heparin (3 kDa) was present at 1.0 mM in both the macromolecule solution in the calorimeter and the ligand solution in the syringe. The ligand, D(II)–D(III) FGFR1, was titrated into the reaction cell which contained bFGF solutions. The data were analyzed with a non-least squares fitting program using the assumption of two sets of noninteracting sites for bFGF as described in the text. [b] See footnote *b* of Table 1 for a description of the binding parameters. Because of the high affinity of the K_1 values, they should be considered apparent K_d's and use the error estimates as an indication of the uncertainty inherent for these measurements (see text).

Table 4: Binding Parameters for Titration of bFGF into Solutions of D(II)–D(III) FGFR1 in the Presence of Low MW Heparin (~3 kDa)[a]

[FGFR1]	[heparin]	site 1			site 2		
in cell (μM)	in cell (mM)	K_1[b] (nM)	n_1	ΔH_1 (kcal/mol)	K_2 (μM)	n_2	ΔH_2 (kcal/mol)
26.2	0.64	1.3 (±1.0)	0.85 (±0.01)	−15.1 (±0.50)	2.4 (±0.9)	1.55 (±0.09)	+14.1 (±1.2)
26.2	0.64	5.3 (±1.7)	0.90 (±0.01)	−18.7 (±0.34)	2.1 (±0.5)	1.23 (±0.05)	+19.0 (±1.1)
27.6	0.62	0.9 (±0.4)	0.93 (±0.01)	−14.5 (±0.29)	2.5 (±0.7)	1.59 (±0.07)	+12.7 (±0.8)
27.6	0.62	2.1 (±0.9)	0.95 (±0.01)	−14.2 (±0.32)	2.7 (±0.7)	1.46 (±0.07)	+14.0 (±1.0)
15.6	0.11	4.2 (±1.6)	1.13 (±0.01)	−9.7 (±0.20)	1.7 (±0.4)	1.47 (±0.06)	+12.1 (±0.8)
15.6	0.11	8.3 (±3.5)	1.15 (±0.01)	−14.7 (±0.31)	2.1 (±0.5)	1.63 (±0.08)	+15.4 (±1.4)
	mean	**3.7 (±2.6)**	**0.99 (±0.11)**	**−14.5 (±2.6)**	**2.3 (±0.3)**	**1.49 (±0.13)**	**+14.6 (±2.3)**

[a] All experiments were performed at 26 °C in 50 mM Hepes buffer at pH 7.5 and 100 mM NaCl. Low MW heparin (~3 kDa) was present at 0.11–0.64 mM in the calorimetric cell with the D(II)–D(III) FGFR1 solutions at 15.6–27.6 μM, as indicated, and the ligand, bFGF, was titrated into the reaction cell. The data were analyzed with a non-least squares fitting program using the assumption of two sets of noninteracting sites for bFGF as described in the text. All six fitting parameters, K_1, n_1, ΔH_1, K_2, n_2, and ΔH_2, were allowed to float for these analyses. These computer fits were made using the "ligand in cell" mode of ORIGIN for deconvolution of the concomitant binding reactions. [b] See footnote *b* of Table 1 for a description of the binding parameters. Because of the high affinity of the K_1 values, they should be considered apparent K_d's and use the error estimates as an indication of the uncertainty inherent for these measurements (see text).

Table 5: Binding Parameters for Titration of D(II)–D(III) FGFR1 into bFGF Solutions in the Presence of 1.5 equiv of Low MW Heparin (3 kDa)/bFGF[a]

[bFGF]	site 1			site 2		
in cell (μM)	K_1[b] (nM)	n_1	ΔH_1 (kcal/mol)	K_2 (μM)	n_2	ΔH_2 (kcal/mol)
28.5	1.7 (±0.7)	0.88 (±0.01)	−18.1 (±0.16)	1.6 (±0.33)	n_1	+3.79 (±0.67)
30.6	5.0 (±1.7)	0.98 (±0.01)	−18.7 (±0.37)	3.1 (±0.55)	n_1	+3.36 (±1.05)
29.3	6.7 (±1.7)	0.93 (±0.01)	−18.6 (±0.37)	1.9 (±0.44)	n_1	+4.65 (±0.67)
25.9	6.3 (±3.9)	1.05 (±0.01)	−14.1 (±0.26)	1.1 (±0.78)	n_1	+4.37 (±0.46)
mean	**4.9 (±2.0)**	**0.96 (±0.06)**	**−17.4 (±1.9)**	**1.9 (±0.7)**	n_1	**+4.04 (±0.50)**

[a] These experiments were performed at 26 °C in 50 mM Hepes at pH 7.5 and 100 mM NaCl. Low MW heparin was present only in the bFGF solution in the calorimetric cell at 1.5 equiv/bFGF. The ligand, D(II)–D(III) FGFR1, was titrated into the reaction cell which contained bFGF solutions. The data were analyzed with a non-least squares fitting program using the assumption of two sets of noninteracting sites for bFGF as described in the text. Only five fitting parameters, K_1, n_1, ΔH_1, K_2, and ΔH_2, were allowed to float for these experiments by fixing $n_1 = n_2$. [b] See footnote *b* of Table 1 for a description of the binding parameters. Because of the high affinity of the K_1 values, they should be considered apparent K_d's and use the error estimates as an indication of the uncertainty inherent for these measurements (see text).

binds with an apparent $K_1 = \sim 5$ nM in an exothermic manner, while the second receptor binds with lower affinity ($K_2 = \sim 2$ μM) in an endothermic manner. The more reliable measurements were from the sequential and isolated binding events as shown in Figure 7 and presented in Table 3. The largest deviations between the two sets of measurements summarized in Tables 3 and 4 are for the magnitude of the endothermic enthalpy change. This may be related to the limitations of curve fitting for unresolved binding events and to the fact that the experiments described in Figure 8 and Table 4 were conducted using 20 injections, while the experiments described in Figure 7 and Table 3 employed 30 injections, thereby allowing a better nonlinear least squares fit.

(C) D(II)–D(III) FGFR1 Titrations of bFGF While Saturating the HS Binding Sites of bFGF with 1.5 equiv of Low MW Heparin. The D(II)–D(III)FGFR1 titrations of bFGF were also conducted with a minimum of 1.5 equiv of low MW heparin (3 kDa)/bFGF present. For example, in a typical experiment the [bFGF] in the calorimetric cell was 28.5 μM and the [heparin (3 kDa)] = 43 μM. Since the affinity of bFGF for low MW heparin is 0.47 μM under similar conditions (Thompson et al., 1994), the addition of 1.5 equiv of low MW heparin will have the effect of saturating the heparin binding site of bFGF and thereby allow an evaluation of the minimum amount of heparin required for the potentiation of the FGF/receptor binding events. After thermal equilibration, a 369 μM D(II)–D(III) FGFR1 solution was titrated into the bFGF/HS solution in 30 × 9.3-μL aliquots spaced at 7 min. The results for this and three other very similar experiments are summarized in Table 5. The presence of HS, at a minimum of 1.5 equiv/bFGF, was also found to increase the binding affinity of FGFR1 to bFGF by ~10 fold over that in the absence of heparin and, importantly, also induce a second FGFR1 molecule to bind to a lower affinity secondary site on

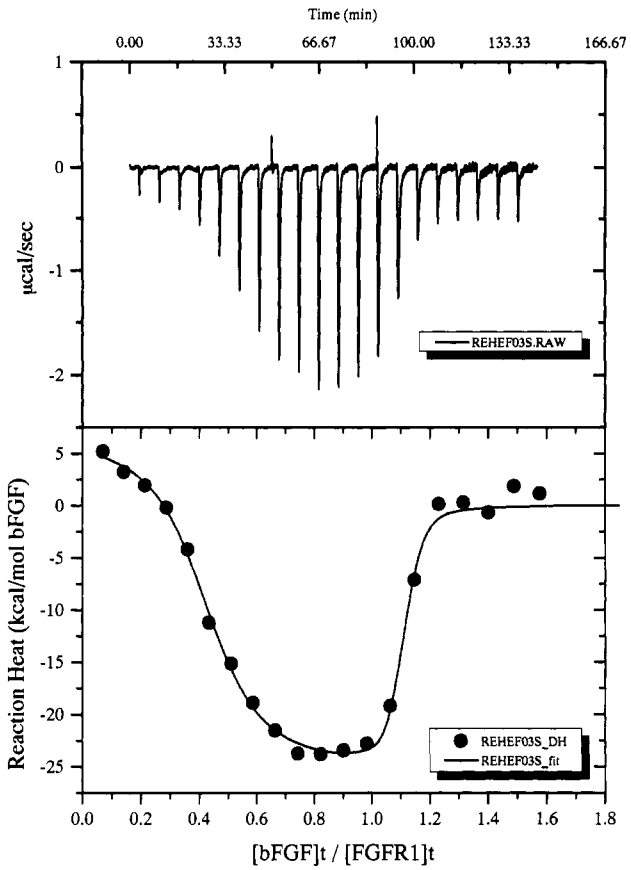

FIGURE 8: bFGF titration of D(II)–D(III) FGFR1 while saturating both receptor and bFGF with low MW heparin. The reverse titration of that in Figure 7 was attempted, and the resulting raw data are shown (top). The resultant binding isotherm for the bFGF titration of D(II)–D(III) FGFR1 in the presence of 0.64 mM HS after integration of the area under each injection peak and subtraction of the blank (bottom). The solid line represents a nonlinear least squares fit of the reaction heat for each injection ($\Delta Q_{(i)}$) with the assumption of two independent sites comprised of the six fitting parameters, n_1, K_1, ΔH_1, n_2, K_2, and ΔH_2, which were all allowed to float during computer iterations (see Materials and Methods). These computer fits were made using the "ligand in cell" mode of ORIGIN for deconvolution of the concomitant binding reactions. This experiment was repeated six times with the [heparin] ranging between 0.11 and 0.64 mM. The results are summarized in Table 4.

bFGF (K_2 = 1.9 ± 0.7 μM) in an entropy-dominated reaction to yield a final quaternary complex of $(FGFR1)_2$/bFGF/HS.

Equilibrium Sedimentation of the D(II)–D(III) FGFR1/bFGF/HS Complex. Measurements of the buoyant molecular weight of the FGFR1/bFGF/HS complex at a mole ratio of 2.0 FGFR1 to 1.0 bFGF in the presence of 1.0 mM low MW heparin were attained using a Beckman analytical ultracentrifuge (XLA). These experiments were conducted under the following conditions: (1) at 30 μM bFGF, 60 μM D(II)–D(III) FGFR1, and 1.0 mM low MW heparin (3 kDa) to simulate the conditions employed for the ITC experiments and to ensure that the bFGF was 15–30-fold above the apparent K_2 measured in these experiments; (2) at 10 μM bFGF, 20 μM D(II)–D(III) FGFR1, and 1.0 mM low MW heparin (3 kDa); (3) at 3.3 μM bFGF, 6.6 μM D(II)–D(III) FGFR1, and 1.0 mM low MW heparin (3 kDa); and (4) at 30 μM D(II)–D(III) FGFR1 and 1.0 mM low MW heparin but in the absence of bFGF. The results, displayed in Table 6, are reported both as buoyant M_b and, using an assumed value of 0.68 for the product of density and protein partial specific volume, as sedimentation M_W in kDa. The low v = 0.68 value is due to the high degree of glycosylation of FGFR1 (20–40%) as described above.

FGFR1 alone sediments as a species of M_W = 45-kDa species, slightly higher than the ~40-kDa estimate by SDS–PAGE analysis and the 39.9 ± 3 kDa estimated by size-exclusion HPLC (see above). The small increase in M_W may be the result of bound HS, since this measurement was made in the presence of 1.0 mM low MW HS.

When bFGF was present in a mole ratio of [FGFR1]t/[bFGF]t = 2.0, the sedimentation M_W was observed to increase to 95.6 kDa under the same conditions. This result is in reasonable agreement with the ITC results since two D(II)–D(III) FGFR1/HS (2 × 45) plus one bFGF (17.4) would be expected to yield a M_W of 107.4 kDa. The slightly smaller M_W for the bFGF/HS-mediated FGFR1 dimer (89% of expected) could be due to a slightly weaker K_2 under the conditions of ultracentrifugation than the 1.2 ± 0.4 μM measured by ITC, which would lead to a higher than expected fraction of lower M_W sedimenting species contributing to the observed average.

The decrease in the sedimentation M_W upon dilution of the FGFR1/bFGF/HS complex from 30 to 3.3 μM is also consistent with the relatively weak binding affinity of the second FGFR1 binding to the 1:1 complex as observed in the ITC experiments reported in Figure 7 and Table 3. The dropoff is steeper than that expected for a 1.2 (±0.4) μM site. This could be due to the fact that although the proteins were diluted ~10 fold, the [HS] was kept constant at 1.0 mM. Under these experimental conditions, HS will compete with increasing effectiveness with the FGFR1/bFGF/HS complex for the binding of the second receptor molecule because $[HS]_t/K_{RH}$ = 10 at 1.0 mM HS, while $[bFGF/FGFR1]_t/K_2$ = 2.8 at 3.3 μM bFGF/FGFR1.

The sedimentation M_W of 45 kDa observed for the FGFR1/bFGF/HS complex diluted to 3.3 μM is smaller than expected for a 50/50 mixture of the free FGFR1/HS of ~45 kDa and the FGFR1/bFGF/HS complex (1:1:1). Assuming all species have the same partial specific volumes, this composition would sediment as its weight average of 53 kDa. It is impossible, however, to attach any significance to this discrepancy without more information about the sedimentation characteristics of individual species.

Biological Competitive Assays of bFGF Binding to D(II)–D(III) FGFR1. Competition assays for measuring the inhibition of D(II)–D(III) FGFR1 (IC_{50}) for the binding of radioactive iodinated bFGF on baby hamster kidney (BHK-21) cells and the separation of high- and low-affinity counts were performed essentially as reported by Moscatelli (1987). The purified receptor was found to inhibit the binding of radioactive labeled ^{125}I bFGF with an IC_{50} = 37.3 (±17.2) nM (no added heparin). These results are in close agreement with those found by ITC.

Three-Dimensional Structural Models of D(II)–D(III) FGFR1. To understand the binary and conditional binding reactions in terms of structural components of FGFR1, a three-dimensional model of D(II)–D(III) FGFR1 was constructed using segment match modeling software described by Levitt (1992). Figure 9A shows the structural model of D(II)–D(III) FGFR1 that resulted when the primary sequence of the D(II) domain of FGFR1 is matched with the primary, secondary, and tertiary structure of the homologous C_H2 domain (17% identity) of the Ig Fc structure (1FC2, PDB; Deisenhofer, 1981).

Similarly, the D(III) domain was modeled using its primary sequence homology with V_H domains, such as the HYHEL-5 antibody structure (2HFL, PDB; Sheriff et al., 1987). The individual D(II) and D(III) domains are each folded into two layers of antiparallel β sheets that embrace a predominantly

Table 6: Equilibrium Sedimentation of FGFR1/bFGF Complexes in the Presence of Low MW Heparin (~3 kDa)[a]

protein in cell	$[bFGF]_t$ (μM)	$[FGFR1]_t/[bFGF]_t$	wt av M_b[b]	wt av M_w (kDa)	reduced χ^2[c]	max no. of FGFR1/bFGF[d]
FGFR1 alone	0.0		14 447 ± 43	45.1	2.0	
FGFR1/bFGF	30.0	2.0	30 586 ± 71	95.6	2.3	2.1
FGFR1/bFGF	10.0	2.0	24 036 ± 56	75.1	1.6	1.7
FGFR1/bFGF	3.3	2.0	14 321 ± 65	44.8	0.8	1.0

[a] These experiments were performed at 20 °C in 50 mM Hepes at pH 7.5, 100 mM NaCl, 1.0 mM DTT, and 1.0 mM low MW heparin (~3 kDa). [b] Single ideal species curve fits were used to determine buoyant molecular weights, M_b. A $\nu = 0.68$ was used for calculations of M_w due to the high degree of glycosylation of FGFR1 (see text). [c] Sedimentation equilibrium optical density gradients were obtained at (in order) 10 000, 8000, and 10 000 rpm. Goodness of fit to the data was assessed by the reduced χ^2 parameter. A value near 1.0 implies that the model fits the data as well as can be expected for assumed Gaussian-distributed errors in the concentration data. Higher values indicate systematic deviations of calculated versus observed values. [d] To account for complex dissociation, the measured M_b was assumed to be a weight average of contributions from three species: $M_b = [C_1M_1^2 + C_2M_2^2 + C_3M_3^2]/[C_1M_1 + C_2M_2 + C_3M_3]$, where C_1 = [FGFR1/bFGF] in the 1:1 complex, $C_2 = [FGFR1]_{free}$, C_3 = [FGFR1/bFGF] in the 2:1 complex, and $C_{tot} = C_1 + C_2 + C_3 = [FGFR1]_{total}$. With the assumption (based on the calorimetric value of 5 nM for the K_d of the 1:1 FGFR1/bFGF complex) that all bFGF is bound at the concentrations used here, the species can be assumed to be in a simple equilibrium relationship: $C_1C_2/C_3 = K_d$. With the further assumption of a fixed stoichiometry of $C_2/C_1 = 1.0$ throughout the centrifugation cell, the weight-average bouyant molecular weight can be expected to vary with total concentrations as $\langle M_b \rangle_w = [M_1^2 + M_2^2 + fM_3^2/(1-f)]/[M_1 + M_2 + fM_3/(1-f)]$, where $f = C_3/[C_t]$ and is the solution to the equation $f^2 + [1 + K_d/C_t]f - 1 = 0$.

hydrophobic core, a structural motif characteristic of constant and variable IgSF domains. The fidelity of the model of D(II) to Ig C_H2 can be judged by an rms deviation of 1.8 Å for the superposition of the 114 equivalent C_α atoms in the β sheets of these two structures. The orientation of the two domains was modeled after the relationship of the two constant domains, C_H2 and C_H3, of the Ig Fc structure, so that the carboxyl terminus of D(II), -PHR-, serves as the interdomain linker that leads into the N-terminus of D(III), -PILA-. This resulted in a structure where the two domains are oriented in the same way that C_H2 and C_H3 domains are aligned in the Ig Fc structure except that the D(III) domain has a V_H-like fold consistent with its closer primary sequence homology with V_H domains (26% identity).

Inspection of the D(II)–D(III) FGFR1 model revealed an elongated cluster of nine cationic residues (seven Lys and two Arg) that are located in the C_H2-like domain D(II) (Figure 9A). Six lysines (residues K6, K9, K10, K18, K21, and K23; numbering system is that of the IgSF homology model which begins at ^{1}WTSP-) are in an extended β turn that involves β strands A and B in the immunoglobulin fold of D(II), while the three remaining cationic residues, R48, K53, and R55, are located in the adjacent β strands C′ and E [see Leahy et al. (1992) for a recent description of Ig β strand folding topography]. This aggregate of positively charged residues was observed in a ~15 × 35 Å shallow cleft formed by the natural twist of the four β strands that comprise the β sheet A, B, E, C′ surface of the D(II) domain (Figure 9A). As expected from this surface charge density, electrostatic potential maps calculated for this FGFR1 model with the program DELPHI (Gilson et al., 1988) revealed that these nine cationic residues focus positive electrostatic potential ($+2k_BT$) to a large part of the solvent exposed A, B, E, C′ β-sheet surface of the D(II) domain model (Figure 9B).

DISCUSSION

The cloning and expression of the extracellular domains D(II)–D(III) of FGFR1 using baculovirus-infected insect cell technology consistently yielded ~15 mg/L culture media when coupled with a bFGF/HS–Sepharose affinity chromatographic recovery method (see Figure 2). These results enabled a biophysical evaluation of the complete binding isotherms for the primary reactants bFGF, HS, and D(II)-D(III) FGFR1, as determined by ITC (Figure 3), under controlled conditions. These individual binding reactions were previously inadequately understood with regard to equilibrium constants, stoichiometry, and structure due, in part, to the prior difficulties in isolating sufficient quantities of each of the purified components and characterizing their binding interactions in controlled cell-free environments. For example, it is commonly believed that bFGF binds to "high affinity" sites on the surface of certain cell lines with an IC_{50} in the range of 0.02–0.20 nM (Klagsbrun & Baird, 1991; Neufeld & Gospodarowicz, 1985), and HS is important for the biological activities of FGF that are triggered by the growth factor binding event to cells (Yayon et al., 1991; Rapraeger et al., 1991). There is, however, uncertainty as to whether HS is obligatory for the bFGF/FGFR1 binding event (Ornitz et al., 1992; Yayon et al., 1991; Klagsbrun & Baird, 1991) and also about how the binding interactions translate into the mechanism of FGF- and HS-mediated biological activities such as mitogenic signal transduction. An attempt to first examine the relevant binary binding reactions for an individual assessment of their intrinsic binding parameters, followed by an examination of the conditional reactions of bFGF and FGFR1 in the presence of HS, is described below.

Binary Binding Reactions for the Reactants, bFGF, FGFR1, and Low MW Heparin. The data in Table 1 and Figures 3–6, together with the information derived from our work with HS binding to bFGF (Thompson et al., 1994), suggest that the relevant binary binding reactions for the FGF system can be dissected into the three reactions comprised of the three primary reactants, bFGF, FGFR1, and HS:

$$\text{FGFR1} + \text{bFGF} \overset{K_{RF} = 41\ \text{nM}}{\Leftrightarrow} \text{FGFR1/bFGF} \quad (1)$$

$$\text{FGFR1} + \text{HS} \overset{K_{RH} = 85\ \mu\text{M}}{\Leftrightarrow} \text{FGFR1/HS} \quad (2)$$

$$\text{bFGF} + \text{HS} \overset{K_{FH} = 470\ \text{nM}}{\Leftrightarrow} \text{bFGF/HS} \quad (3)$$

(A) Intrinsic Binding of bFGF to FGFR1 in the Absence of HS. Reaction 1 is the intrinsic binding affinity of bFGF for FGFR1, in the absence of HS. The results summarized in Table 1 show the stoichiometry of this reaction to be 1:1 over an 8-fold range of [protein] with an observed dissociation constant K_{RF} = 41 (±12) nM when bFGF is incrementally titrated into D(II)–D(III) FGFR1 solutions in the absence of HS (Table 1A). This translates into an observed free energy of binding of $\Delta G° = -10.2$ (±0.2) kcal/mol when calculated using $\Delta G° = -RT \ln K_a$.

Nearly identical results were obtained (i.e., $n = 0.99$, and an observed $\Delta G° = -10.0$ kcal/mol) when the order of addition of the reactants was reversed, where D(II)–D(III) FGFR1 is titrated incrementally into bFGF solutions in the absence of HS under otherwise identical conditions (Table 1B). The

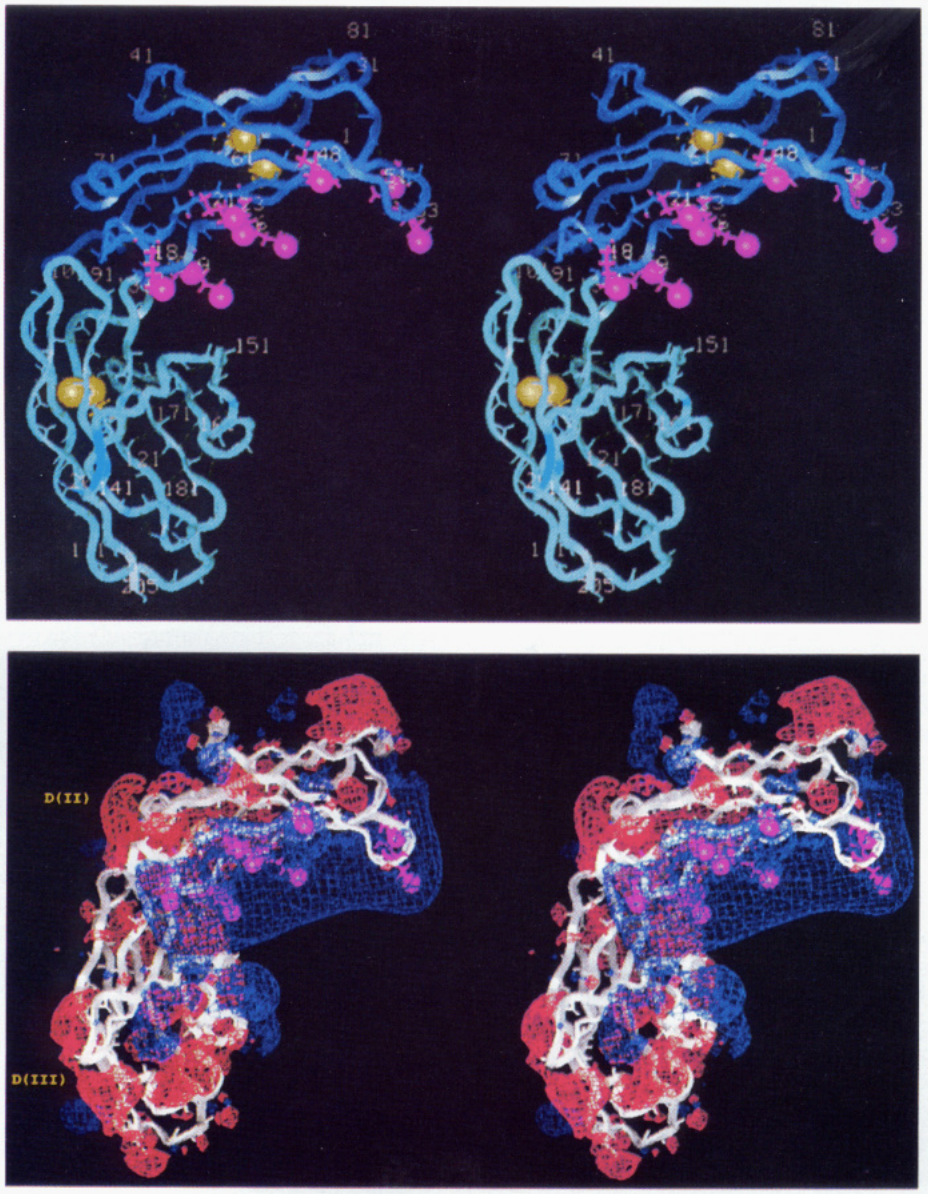

FIGURE 9: Stereoviews of a three-dimensional model of D(II)–D(III) FGFR1. (A, top) A homology model of D(II)–D(III) FGFR1 was built using the segment match modeling program, SEGMOD, of Levitt (1992) as described in the text. The backbone of FGFR1 is shown as a ribbon with the D(II) domain (dark blue) at the top and the membrane proximal D(III) domain (light blue) at the bottom. A cluster of nine cationic residues is shown with their side-chain atoms colored purple and the cationic atoms, N^{ζ} (Lys) and N^{ϵ} (Arg), highlighted in CPK. The side chains correspond to residues K6, K9, K10, K18, K21, K23, R48, K53, and R55 in the model which uses the numbering system relative to the first residue of the Ig homology fold, i.e., ^{1}WTSP-. The yellow spheres are the S^{γ} atoms of the conserved disulfide linkages (24–76 and 123–187) characteristic of the Ig constant and variable domain folding motifs. Hydrogen bonds are shown as dotted green lines. (B, bottom) Computation of an electrostatic potential map for the D(II)–D(III) FGFR1 model. An electrostatic potential map (total electrostatic energy plus grid) was calculated for the D(II)–D(III) FGFR1 model using the program DELPHI (Gilson et al., 1988) interfaced with INSIGHTII v2.3.0 (BioSym). This program uses the Poisson–Boltzmann equation to compute electrostatic forces on solvated molecules. Parameters employed for the FGFR1 model calculation were as follows: solute dielectric was set at 2 and solvent dielectric was set at 80, while the ionic strength was assigned to a physiological 0.145. The protein atomic potentials were assigned using the AMBER force field (Weiner & Kollman, 1981) while the pH was fixed to 7.5. A grid of 65 × 63 × 49 Å with a grid step of 1.3 Å/grid point was employed for the calculation after a full Coulombic boundary condition was assigned. Two electrostatic energy levels are shown in this figure: $+2k_BT$ (blue) and $-2k_BT$ (red). The nine cationic residues responsible for the large elongated positive potential localized to the solvent-exposed A, B, E, C′ β sheet are the same residues found clustered in (A).

close agreement for the reversed order of reactant addition indicates that the binding of bFGF to FGFR1 is a simple binary reaction characterized by a single association constant and does *not* require the presence of heparin, heparan sulfate, or HSPG. Furthermore, the large free energy of binding for this reaction, $\Delta G° = -10.2\ (\pm 0.2)$ kcal/mol, identifies reaction 1 as the central binding reaction for the FGF system.

The results for the intrinsic bFGF and D(II)–D(III) FGFR1 binding in the absence of HS are in agreement with those of Keifer et al. (1991) and Bergonzoni et al. (1992), who both reported IC_{50} measurements of 5–10 nM for the three IgSF domain version, D(I)–D(II)–D(III), of the extracellular binding region of FGFR1 in the absence of HS. The small increase in binding affinities observed by these authors could be due to the presence of D(I) for their constructs of FGFR1 or, alternatively, due to small buffer-related effects on the assay (see Table 2).

(B) Intrinsic Binding of HS to FGFR1 in the Absence of bFGF. The second fundamental binary binding reaction for the FGF system is the intrinsic binding affinity of FGFR1 for HS, in the absence of bFGF, reaction 2. Heparin binding to FGFR1 was also investigated by ITC through incremental addition of low MW HS into D(II)–D(III) FGFR1 solutions (Figure 4). The results of these studies revealed that the

stoichiometry of this reaction is 1.39 (±0.06) HS to 1.0 D(II)–D(III) FGFR1 (using MW = 3000 for low MW HS) with an observed dissociation constant of K_{RH} = 104 (±17) μM. Similar results were obtained for RD Heparin 5000 (Figure 5).

Although the binding affinity of reaction 2 was found to be relatively weak in comparison to other more familiar HS binding sites such as thrombin (Olson et al., 1991), antithrombin III (Olson & Björk, 1991), and bFGF (see below), the HS binding site of D(II)–D(III) FGFR1 is believed to be biologically relevant because of the high expression levels of HSPG on the surface of cells that coexpress FGFR1. Yanagishita and Hascall (1992) have found that typical expression of HSPG is in the range of 10^5–10^6 copies per cell. As pointed out by Brandts and Jacobson (1983) in their thermodynamic treatment of membrane receptor clustering mechanisms for transmembrane signal transduction, the mass law dependence for reactions involving membrane receptors is more conveniently treated using two-dimensional leaflet mole fractions, $X_R = N_R/(0.5N_L + N_R)$, as the concentration units, where N_R = number of embedded receptor molecules and N_L = number of lipid molecules (0.5 is due to the bilayer nature of biological membranes) since the receptors can be assumed to have no significant degrees of freedom in the Z-direction perpendicular to the plane of the bilayer. For 10^6 copies of a membrane receptor on the surface of an erythrocyte-sized cell, the bulk concentration of receptor in the membrane expressed in terms of two-dimensional leaflet mole fractions was estimated to be $X_R = 5 \times 10^{-3}$ (Brandts & Jacobson, 1983). Therefore, a K_{RH} = 85–104 μM binding affinity measured *in vitro* in three-dimensional concentration units for HS binding to D(II)–D(III) FGFR1 is believed to be relevant for cases where HSPG-like surface molecules are expressed to such a high level that the effective two-dimensional concentrations can be estimated to be 5–50-fold above the observed K_d.[9] Similar calculations for the estimated 2000 copies of the FGFR1 expressed on the surface of the same cell lines yield an effective two-dimensional leaflet mole fraction of $X_R = 1 \times 10^{-5}$ for FGFR1.

(C) Pentosan Polysulfate Binding to D(II)–D(III) FGFR1. The binding of PPS to D(II)–D(III) FGFR1 (Figure 6) is intriguing since this sulfated oligosaccharide is a well-known inhibitor of angiogenesis and is currently being investigated for the treatment of breast cancer (Lippman, 1993; Harris et al., 1992) and AIDS-related Kaposi's skin cancer (Wellstein et al., 1991; Nakamura et al., 1992). The mechanism of action of PPS was presumed to be through the competitive inhibition of HSPG binding to FGF (reaction 3) and subsequent interference with the previously held view that HSPG/FGF complex formation is required for binding to FGFR1, a view that now appears to be untenable when the results in Table 1 are considered. The observations described above for reaction 1, together with the observation that PPS binds to FGFR1 with a 10-fold higher affinity than HS [K_d = 10.9 (±3.5) μM], however, may provide an opportunity to reexamine the mechanism of action of this sulfated oligosaccharide and other related angiogenesis inhibitors such as the sulfated polysaccharide peptidoglycan SP-PG (Nakamura et al., 1992) and the sulfated naphthalene, suramin (Harris et al., 1992). In this regard, it has been reported that PPS inhibits growth of both AIDS-Kaposi sarcoma cells and normal human endothelial cells from umbilical vein (H-UVE) with IC_{50}'s of 2 and 8 μM, respectively (Nakamura et al., 1992). These growth inhibition data are in close agreement with the observed binding affinity of PPS to FGFR1 shown in Figure 6.

(D) Intrinsic Binding of HS to bFGF in the Absence of FGFR1. The third fundamental binary binding reaction, reaction 3, is the intrinsic binding affinity of bFGF for HS, in the absence of FGFR1. A detailed characterization of this reaction through the use of molecular modeling of docked heparin/bFGF interactions and site-directed mutagenesis of bFGF, in addition to isothermal titrating calorimetry, has been reported (Thompson et al., 1994). Briefly, the wild-type bFGF was found to bind to low MW heparin (~3 kDa) to yield a K_{FH} = 470 (±20) nM when titrated under conditions identical to those in Tables 1 and 2, i.e., 50 mM Hepes–NaOH, pH 7.5, 0.10 M NaCl, 1.0 mM DTT, and 26 °C. The value of the equilibrium constant was also found to be independent of the order of addition of the two reactants.

Conditional Reactions of bFGF and FGFR1 in the Presence of Low MW Heparin. The conditional reactions of bFGF and FGFR1 in the presence of heparin were examined under circumstances that saturate only the bFGF heparin site (1.5 equiv of HS/bFGF) or saturate the HS binding sites of both bFGF and FGFR1 (1.0 mM HS). Both 3- and 5-kDa low MW heparin were found to give ~10-fold increase in affinity for FGFR1 binding to bFGF (K_1 = 5 nM) when [HS] = 1.0 mM, relative to the reaction with no heparin (Figure 7, Tables 3 and 4). The presence of HS, at a minimum of 1.5 equiv/bFGF, was found to induce a second FGFR1 molecule to bind to a lower affinity secondary site on FGFR1/bFGF/HS (K_2 = 1.9 ± 0.7 μM) in an entropy-dominated reaction to yield a final quaternary complex of $(FGFR1)_2$/bFGF/HS. Equilibrium sedimentation experiments were found to be consistent with this result when conducted at $[FGFR1]_t/[bFGF]_t = 2.0$ in the presence of 1.0 mM low MW heparin (~3 kDa) (Table 6). The titrations of bFGF and FGFR1 in both directions in the presence of saturating levels of heparin are in close agreement (Tables 4 and 5) and strongly suggest that heparin binding events on both of these proteins induce bFGF-mediated receptor dimerization.

The endothermic nature of the second receptor binding event observed for both 1.0 mM heparin and the minimum 1.5 equiv/bFGF can be explained in terms of the burial of a large nonpolar surface area upon binding to form the quaternary complex $(FGFR1)_2$/bFGF/HS or quinary complex $(FGFR1)_2$/bFGF/$(HS)_2$ as might be expected for protein/protein interactions that involved the IgSF (see below).

Allosteric Modulation of the Multivalent Binding Equilibria of FGFR1, bFGF, and Heparin. The dissection of the binding reactions of the three primary reactants into the three fundamental binary reactions (1–3) reveals that each reactant is multivalent: FGFR1 binds growth factor *and* HS, bFGF binds receptor *and* HS, and HS binds FGFR1 *and* bFGF. The multivalent nature of each primary reactant suggests that many unanswered questions for this growth factor system that relate to the role of heparin in high-affinity binding and the mechanism of mitogenic signal transduction can be understood in terms of well-studied classical multiple ligand binding mechanisms (Wyman, 1964; Weber, 1975). In the presence of heparin, at a minimum of 1.5 equiv/bFGF, there is an ~10-fold potentiation of reaction 1 and the induction of a fourth reaction, which is the binding of a second molecule of FGFR1 to yield a quaternary complex:

$$\text{FGFR1/bFGF/HS} + \text{FGFR1} \overset{\alpha\beta\gamma K_{RR} = 1.9\ \mu M}{\Longleftrightarrow} (\text{FGFR1})_2\text{/bFGF/HS} \quad (4)$$

[9] This calculation assumes one FGFR1 binding site per HSPG, which is most likely an underestimate depending on how many sites can be accommodated per HS chain with a typical MW of 30 000. The evidence provided in Figures 4 and 5 is that there is one FGFR1 site per ~3–5 kDa of HS.

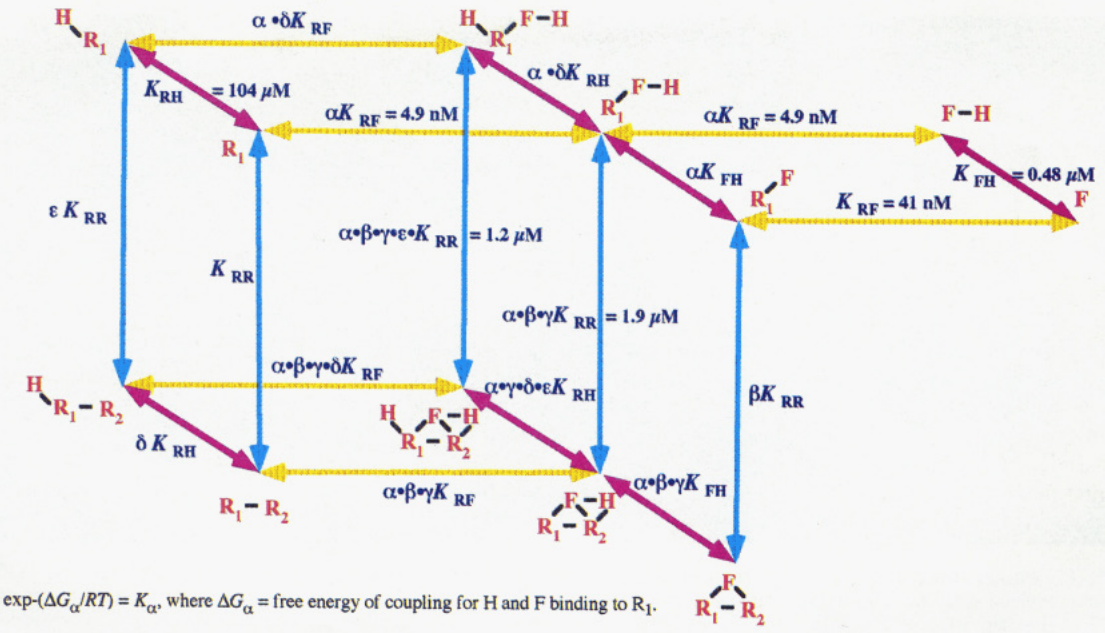

$\alpha = \exp[-(\Delta G_\alpha/RT)] = K_\alpha$, where ΔG_α = free energy of coupling for H and F binding to R_1.

$\beta = \exp[-(\Delta G_\beta/RT)] = K_\beta$, where ΔG_β = free energy of coupling of F and R_2 binding to R_1.

$\gamma = \exp[-(\Delta G_\gamma/RT)] = K_\gamma$, where ΔG_γ = free energy of coupling for H and R_1F binding to R_2.

$\delta = \exp[-(\Delta G_\delta/RT)] = K_\delta$, where ΔG_δ = free energy of coupling for H and FH binding to R_1.

$\varepsilon = \exp[-(\Delta G_\varepsilon/RT)] = K_\varepsilon$, where ΔG_ε = free energy of coupling for H and R_2 binding to R_1.

FIGURE 10: Allosteric modulation of the multivalent binding equilibria of FGFR1, bFGF, and heparin. This schematic illustrates how the multiple ligand binding equilibria of the three reactants of the FGF system can be understood in terms of an allosteric mechanism for the dimerization of the FGF receptor, where R = FGFR1 ($R_1 = R_2$; the subscripts are used to denote the first and second receptor to bind to the growth factor), F = bFGF, and H = low MW heparin (~3 or 5 kDa). The three binary equilibrium dissociation constants, K_{RF}, K_{RH}, and K_{FH}, characterize the binding of R to F, R to H, and F to H, respectively, as discussed in the text. The reactions are color coded so that all R/F binding reactions are in yellow and lie in the *X*-direction, while all heparin binding reactions, either F/H or R/H, are in purple and lie in the *Z*-direction. A fourth binary binding reaction is postulated, K_{RR}, which is the dimerization of R to yield R_1–R_2, in the absence of all ligands. All the receptor dimerization reactions are in blue and lie in the *Y*-direction. The K_{RR} reaction is assumed to be a very weak association and undetectable in the absence of other ligands but was observed in the presence of both the ligands, F and H. This can be understood if the binding of each of the ligands modifies the affinity of the other ligands by a certain factor, and the principle of microscopic reversibility suggests five such interaction factors: α, β, γ, δ, and ϵ. For example, it was observed that H potentiates the binding of F to its receptor R, by ~10-fold, so that the reaction of R and FH is characterized by $\alpha K_{RF} = 4.9 \pm 2.0$ nM, where $\alpha = \exp[-(\Delta G_\alpha/RT)] = K_\alpha = \sim 10$ and $\Delta G_\alpha = \sim -1.4$ kcal/mol = free energy of coupling for bFGF and H binding to R_1 (Weber, 1975). Similarly, the binding of FH to R_1 (1.5 equiv of H/F) is believed to potentiate the binding of R_1 to a second receptor, R_2, so that the resultant receptor dimerization is characterized by $\alpha\beta\gamma K_{RR} = 1.9$ (± 0.7) μM, where $\beta = \exp[-(\Delta G_\beta/RT)] = K_\beta$ and ΔG_β = free energy of coupling for bFGF and R_2 binding to R_1 and where $\gamma = \exp[-(\Delta G_\gamma/RT)] = K_\gamma$ and ΔG_γ = free energy of coupling for H (bound to bFGF) and R_1F binding to R_2. Additional interaction factors that may play a role for the mechanism of receptor dimerization when the [HS] = 1.0 mM are $\delta = \exp[-(\Delta G_\delta/RT)] = K_\delta$, where ΔG_δ = free energy of coupling for H and bFGF/H binding to R_1, and $\epsilon = \exp[-(\Delta G_\epsilon/RT)] = K_\epsilon$, where ΔG_ϵ = free energy of coupling for H and R_2 binding to R_1.

An allosteric mechanism that attempts to explain how FGF and HS together induce the dimerization of FGFR1, reaction 4, is shown in Figure 10. The foundation of this mechanism lies with the three binary equilibrium dissociation constants, K_{RF}, K_{RH}, and K_{FH}, as discussed above. A fourth binary binding reaction is postulated, K_{RR}, which is the dimerization of FGFR1 to yield R_1–R_2, in the absence of all ligands ($R_1 = R_2$; the subscripts are used to indicate the first and second receptor to bind to the ligand, FGF/HS). This reaction is assumed to be a very weak association and undetectable in the absence of other ligands at [FGFR1] $\approx$ 30 μM but was observed in the presence of both the ligands, F and H. The reason for this shift in equilibrium comes from the evidence that the binding of each of the ligands modifies the affinity of the other ligands by a certain factor, and the principle of microscopic reversibility suggests five such interaction factors: α, β, γ, δ, and ϵ. This is a consequence of the trivalent binding preferences of F, the trivalent binding characteristics of R, and the bivalent binding properties of H.

For example, if one begins with growth factor, F, in Figure 10, this reactant has a choice: it can bind to H, shown as the purple reaction characterized by $K_{FH} = 0.48$ μM, leading to the formation of F–H; or it can bind to R_1 shown as the yellow reaction characterized by $K_{RF} = 41$ nM, leading to the binary complex, R_1-F. The binary complexes, F–H and R_1–F, can then react with R_1, or H, respectively, to yield the same ternary complex R_1–F–H. It was observed that H increases the binding affinity of F to its receptor R, by ~10-fold, so that the reaction of R and FH is characterized by $\alpha K_{RF} = 4.9 \pm 2.0$ nM, where $\alpha = \exp[-(\Delta G_\alpha/RT)] = K_\alpha = \sim 10$ and $\Delta G_\alpha = \sim -1.4$ kcal/mol = free energy of coupling for bFGF and H binding to R_1 (Weber, 1975). The principle of microscopic reversibility, implicit in the linkage of multivalent binding reactions, suggests that R should increase the binding affinity of F to H by the same interaction factor, α, to yield αK_{FH}. It is also possible to arrive at the ternary complex R_1–F–H in Figure 10 by starting at R_1 and reacting with FH, shown as the yellow reaction also characterized by $\alpha K_{RF} = 4.9 \pm 2.0$ nM.

Similarly, the binding of FH to R_1 (1.5 equiv H/F) is believed to increase the binding affinity of R_1 to a second receptor, R_2, so that the resultant receptor dimerization is characterized by $\alpha\beta\gamma K_{RR} = 1.9 \pm 0.7$ μM, where $\beta = \exp[-(\Delta G_\beta/RT)] = K_\beta$ and ΔG_β = free energy of coupling for bFGF and R_2 binding to R_1 and where $\gamma = \exp[-(\Delta G_\gamma/RT)]$

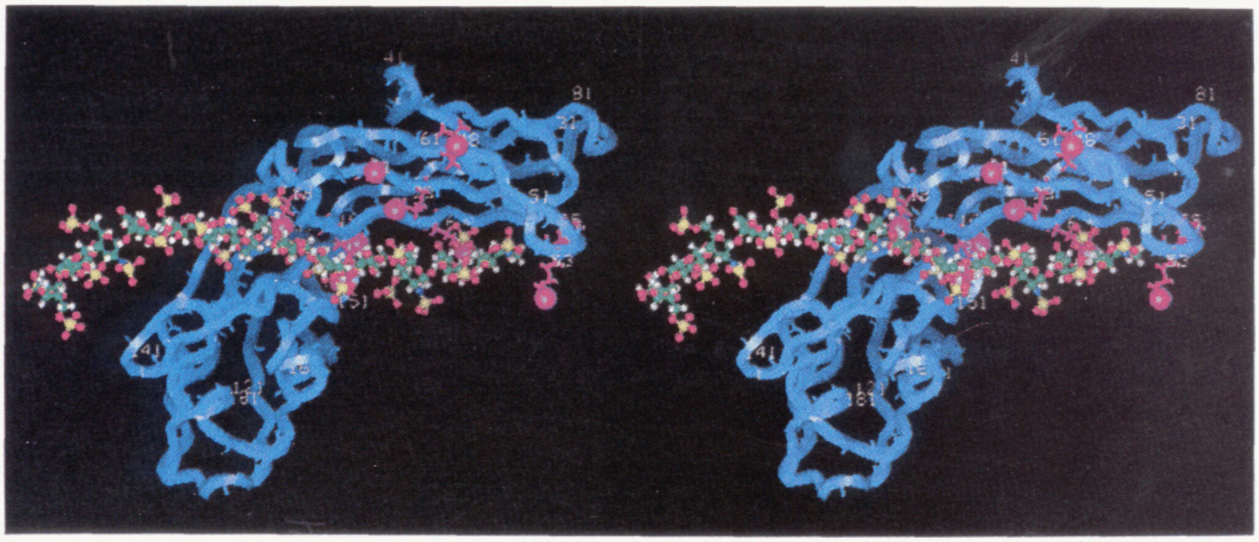

FIGURE 11: Preliminary docking of a low MW heparin model to the locus of positive electrostatic potential of the D(II)–D(III) FGFR1 model. A 13 monosaccharide sized heparin model was constructed to approximate a low MW heparin that is intermediate between that of heparin 3000 and RD Heparin 5000 with a MW = 4400 (see text). The atoms of this sulfated oligosaccharide model are color coded: C, green; H, white; N, blue; O, red; and S, yellow. The helical conformation of the heparin model is that obtained after energy minimization using DISCOVER within INSIGHTII. The negatively charged ligand is oriented so that an ~5-Å translation in the *Y*-direction will place it into the locus of positive electrostatic potential identified in Figure 9B for the D(II)–D(III) FGFR1 model.

$= K_\gamma$ and ΔG_γ = free energy of coupling for H (bound to bFGF) and R_1F binding to R_2. It is not known to what extent β and γ each potentiate the receptor dimerization reaction, K_{RR}, but if the free energies of coupling are assumed to be additive and roughly equal, then the interaction factors are $\alpha = \beta = \gamma = \sim 10$, and an ~1000-fold increase in K_{RR} would be expected over that detectable in the absence of any ligands. Since these three interaction factors, α, β, and γ, are all that is required to account for the reactions that lead to the quaternary complex, $(FGFR1)_2$/bFGF/HS, observed in the presence of 1.5 equiv of HS/bFGF, we believe that they are the most important of the five. This is supported by the observation that $\alpha\beta\gamma K_{RR} = 1.9 \pm 0.7$ μM, observed in the presence of 1.5 equiv/bFGF, is not greatly increased when 1.0 mM heparin is present; i.e., $\alpha\beta\gamma\epsilon K_{RR} = 1.2 \pm 0.4$ μM. This suggests that the interaction coupling factors, δ and ϵ, are not as important for receptor dimerization: $\delta = \exp[-(\Delta G_\delta/RT)] = K_\delta$, where ΔG_δ = free energy of coupling for H and bFGF/H binding to R_1, and $\epsilon = \exp[-(\Delta G_\epsilon/RT)] = K_\epsilon$, where ΔG_ϵ = free energy of coupling for H and R_2 binding to R_1. HS-induced receptor dimerization was not observed in the absence of bFGF, just as bFGF-induced receptor dimerization was not observed in the absence of HS under the conditions employed here, but may occur at high [protein].

The thermodynamic driving force for receptor dimerization can therefore be understood in terms of allosteric multivalent binding reactions that allow for the cooperative energetic coupling of heparin binding reactions on FGFR1 and bFGF, reactions 2 and 3, with growth factor/receptor binding events, reactions 1 and 4. This mechanism is not unlike those mechanisms invoked to explain the effects of one ligand binding on another in other classic multivalent protein systems (Wyman, 1964; Weber, 1975) and is similar to that recently used to explain the dual agonist activation of *N*-methyl-D-aspartate receptors (Marvizón & Baudry, 1993). The energetic coupling of reactions 2 and 3 through a cooperative mechanism with the bFGF/FGFR1 binding events, as shown in Figure 10, is nicely compatible with the observations derived from cell biology experiments that HSPG is required for the biological activity of bFGF (Rapraeger et al., 1991; Yayon et al., 1991). Moreover, the mechanism proposed in Figure 10 is also in agreement with other reports that the FGFR intracellular tyrosine kinase domains become juxtaposed in a manner that leads to cross-phosphorylation (Bellot et al., 1991; Ullrich & Schlessinger, 1990; Ueno et al., 1992). Thus, the initiation of FGF-mediated signal transduction is analogous to the mechanism observed for the dimerization of the human growth hormone (HGH) receptor mediated by HGH (Cunningham et al., 1991; De Vos et al., 1992) with the important difference that the FGF system has recruited HSPG to act as a coagonist.

Correlation of Binding Reactions with Structural Models of D(II)–D(III) FGFR1. A three-dimensional model of D(II)–D(III) FGFR1 was constructed using segment match modeling software described by Levitt (1992) and is shown in Figure 9. This enabled a correlation of the binary and conditional binding reactions with structural components of FGFR1. An appreciation of how D(II)–D(III) FGFR1 might accommodate an HS-like ligand is shown in Figure 11, which compares the FGFR1 model side by side with a structural model of low MW heparin. In this case a 13 monosaccharide sized heparin model was constructed to approximate a low MW heparin that is intermediate between that of heparin 3000 and RD Heparin 5000, $GlcNSO_3$-(6-OSO_3)-α(1→4)-IdoA-α(1→4)-$GlcNSO_3$-(2-OSO_3)-(6-OSO_3)-α(1→4)-GlcUA-(3-OSO_3)-α(1→4)-$GlcNSO_3$-(6-OSO_3)-α(1→4)-IdoA-α(1→4)-$GlcNSO_3$-(2-OSO_3)-(6-OSO_3)-α(1→4)-GlcUA-(3-OSO_3)-α(1→4)-$GlcNSO_3$-(6-OSO_3)-α(1→4)-IdoA-α(1→4)-$GlcNSO_3$-(2-OSO_3)-(6-OSO_3)-α(1→4)-GlcUA-(3-OSO_3)-α(1→4)-$GlcNSO_3$-(6-OSO_3)-OMe, where $GlcNSO_3$-(6-OSO_3) is D-glucosamine-*N*-6-disulfate, IdoA is L-iduronic acid, GlcUA is D-glucuronic acid, and the sulfate substituents are numbered using the IUPAC convention for carbohydrates. The modeled HS is essentially the combination of two identical copies of the synthetic pentasaccharide heparin analog that has been well characterized for its binding to antithrombin III (Petitou et al., 1991; Grootenhuis & van Boeckel, 1991) but connected by a trisaccharide linker, -IdoA-α(1→4)-$GlcNSO_3$-(2-OSO_3)-(6-OSO_3)-α(1→4)-GlcUA-(3-OSO_3)-. The molecular weight of this 13-monosaccharide heparin model is 4420 (Na^+ salt) and ~60 Å in length. The helical twist for the heparin model was an outcome of energy minimization to relax the structure around the ψ and ϕ angles of the 1,4 linkages and also to optimize the electrostatic

repulsion of the $-SO_3^-$ and $-COO^-$ groups after computer synthesis. This helical structure is consistent with the known single-stranded helical nature for related glycosaminoglycans, such as dermatan sulfate, studied by X-ray diffraction (Arnott & Mitra, 1984; Mitra et al., 1983).

The juxtaposition of this 13-monosaccharide model of low MW HS near the clustered cationic groups at the A, B, E, C′ β sheet reveals how a translation of ~5 Å in the +Y-direction would dock the HS ligand against the A, B, E, C′ β surface of D(II) in such a way that would complement the positive electrostatic potential map in Figure 9B. In this binding configuration, six or seven of the HS monosaccharides would interact with the D(II) binding cleft, but the remaining six or seven would be sterically precluded for binding another FGFR1 molecule. This observation, based on the poised structural models of Figure 11, is consistent with the 1:1 binding stoichiometry observed for the 10 monosaccharide sized heparin 3000, the 15 monosaccharide sized, RD Heparin 5000, and the 12 monosaccharide sized pentosan polysulfate (MW ~4500) reported for the binding experiments of Figures 4–6.

An elongated clustering of positively charged residues that focus positive electrostatic potential at protein surfaces has the capability to interact with opposite sides of the carbohydrate in a two-sided binding mode. This heparin binding structural motif has also been observed for the HS binding proteins thrombin (Bode et al., 1992), antithrombin III (Grootenhuis & van Boeckel, 1991), and bFGF (Zhang et al., 1991; Thompson et al., 1994) and strongly suggests that these nine FGFR1 cationic residues, discussed above, constitute the greater part of the HS binding domain of FGFR1. Identification of sulfated proteoglycan binding regions in other proteins for which no X-ray or NMR information is available has also been successfully employed by Sali et al. (1993) through a similar strategy of homology modeling and electrostatic potential calculations.

During the course of these investigations the existence of a heparin binding site for FGFR1 was identified in the D(II) domain using peptide mapping and site-directed mutagenesis of FGFR1 (Kan et al., 1993). The binding data and modeling exercises described here are consistent with the results of these authors. When comparing the location of the clustered nine cationic residues in Figure 9 with the peptide sequence K18K, NH_2-KMEKKLHAVPAAKTVKFK-COOH, identified by Kan et al. (1993) as comprising at least part of the heparin binding site of FGFR1, we found that six of the lysines in the model, residues K6, K9, K10, K18, K21, and K23 located in the A and B β strands of domain D(II), corresponded to the six lysine residues in the K18K peptide. The close agreement between the results of Kan et al. (1993) and the electrostatic potential calculations for the three-dimensional structural model of FGFR1 further supports the assertion that the heparin binding site of FGFR1 is fairly accurately represented in Figures 9 and 11.

The feasibility of side-by-side adjacent binding of bFGF and FGFR1 to a heparin polymer of sufficient length to bridge the growth factor and receptor was explored through docking simulations that aligned the HS binding domains of these two proteins. The HS binding domain of bFGF was recently defined by a combination of molecular modeling, site-directed mutagenesis, and isothermal titrating calorimetry (Thompson et al., 1994). Approximately 95% of the binding free energy for the bFGF/HS interaction, K_{FH}, was accounted for through individual substitutions of eleven residues, K26, N27, R81, K119, R120, T121, Q123, K125, K129, Q134, and K135, of bFGF to alanine residues. The locations of many of these residues were consistent with those adjacent to bound sulfate anions that cocrystallized with bFGF (Zhang et al., 1991; Eriksson et al., 1991) and also the site of sucrose octasulfate binding (Zhu et al., 1993). Docking simulations of FGFR1 and bFGF revealed that the heparin binding domains of each of these proteins could be aligned to yield a continuous stretch of heparin binding residues of ~60 Å that transverse both proteins (Figure 12). The 13 monosaccharide sized heparin model that mimics low MW heparin is also shown poised to interact with this continuous reach of heparin binding residues without any need to perturb the modeled HS helical conformation. This simulation reveals that side-by-side adjacent binding of growth factor and receptor is quite reasonable for HS of ~10–15 monosaccharide length.

Concomitant with the heparin binding domain alignment of FGF and FGFR1, it was also possible to simultaneously juxtapose the putative receptor binding loop of bFGF, ^{110}KYTSW^{114} (Baird et al., 1988), against the exterior D(II)/D(III) domain elbow junction of FGFR1 (Figure 12), which is analogous to the protein A binding site of the homology-matched IgFc. This locus (white surface of Figure 12) is the most likely site for FGF binding, given the sequence comparisons between D(II) and Ig C_H2 and the X-ray structural evidence for the involvement of the exterior elbow junction for the HGH/HGH receptor interaction (De Vos et al., 1992). The alignment of the heparin binding residues for FGF and FGFR1, together with the docking of the ^{110}KYTSW^{114} loop of bFGF (Baird et al., 1988) against the proposed FGF binding site of FGFR1, thereby provides the means for a binary docking process that results in a two-point landing of the two proteins and eliminates many alternative orientations (Stoddard & Koshland, 1992). This outcome is instructive, since it suggests an explanation for the manner in which two adjacent molecular recognition sites of bFGF, the heparin binding domain and the putative receptor binding loop (Baird et al., 1988), can collaborate with their counterparts on FGFR1 to produce a bFGF/FGFR1/HS complex and thereby provide a structural explanation for the experimental observation that the HS (13 monosaccharide sized) binding events on FGFR1 and bFGF, reactions 2 and 3, are energetically coupled to growth factor/receptor binding events, reactions 1 and 4. The apparent greater dependence on the presence of HS for reaction 4 over reaction 1 may suggest that the ^{110}KYTSW^{114}/D(II)–D(III) FGFR1 interface is involved with the second receptor binding event (Figure 10). Characterization of the binding interface, ^{110}KYTSW^{114}/D(II)–D(III) FGFR1, by site-directed mutagenesis (Springer et al., unpublished results) further supports the belief that this represents the binding interface that is the product of the second receptor binding event, reaction 4, characterized by $\alpha\beta\gamma K_{RR}$ = 1.9 μM, in the receptor dimerization mechanism (Figure 10).

A second D(II)–D(III) FGFR1 moiety added to the ternary complex of Figure 12 revealed how the three reactants of the FGF system were assembled to satisfy all of the multivalent binding results but still remain within the framework of the identified structural binding components of the X-ray structure of bFGF and the homology model of D(II)–D(III) FGFR1 (Figure 13). This simulation was also a binary docking process in that it employed a two-point landing of the proposed FGF binding site of FGFR1 (white surface) onto a second receptor binding site of bFGF (red surface ~180° from ^{110}KYTSW^{114} on left also identified by site-directed mutagenesis mapping; Springer et al., unpublished results), and a concomitant D(III)/D(III) dimerization (green surfaces) to be consistent with the results for the HGH receptor (De Vos et al., 1992). The quaternary complex of FGFR1, bFGF, and HS that results

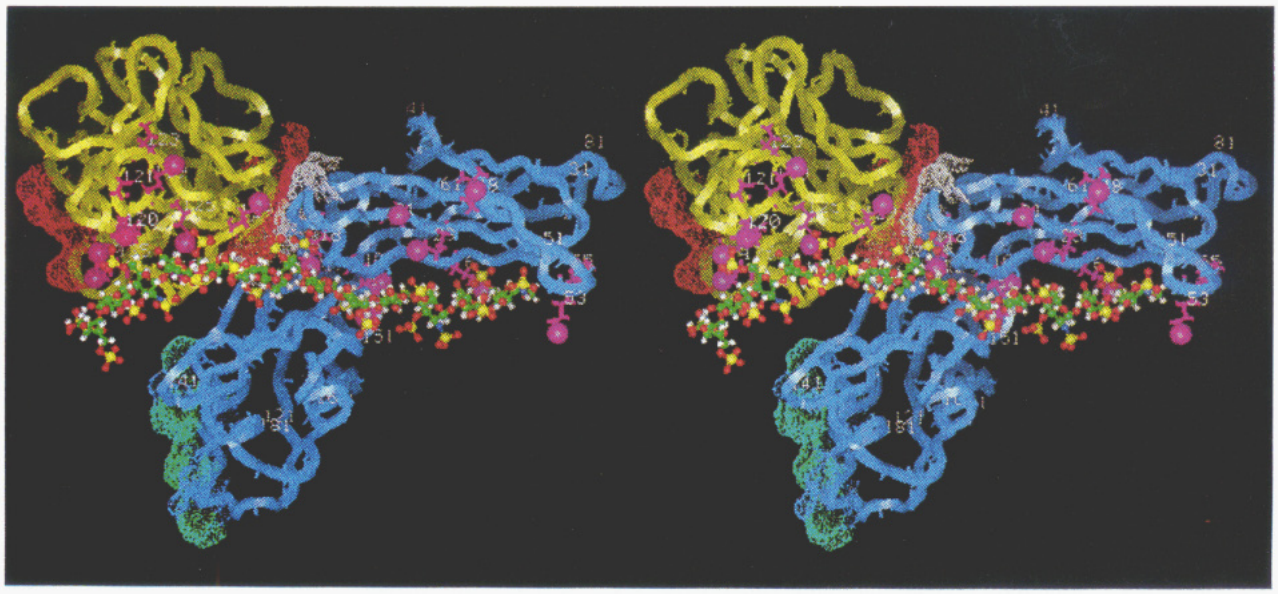

FIGURE 12: Stereoview of a model for the alignment of the heparin binding domains of D(II)–D(III) FGFR1 and bFGF. The heparin binding domain of bFGF was found by Thompson et al. (1994) to be comprised of 11 residues, K26, N27, R81, K119, R120, T121, Q123, K125, K129, Q134, and K135, whose side-chain atoms are colored purple and the cationic atoms, N^{ζ} (Lys) and N^{ϵ} (Arg), highlighted in CPK. A yellow ribbon represents the remainder of the bFGF structure (Zhang et al., 1991). These residues are shown as they were found to interact with a docked pentasaccharide heparin model as described by Thompson et al. (1994). This heparin binding site for bFGF was then aligned with the heparin binding site for D(II)–D(III) FGFR1 as described in Figures 9 and 11. This resulted in the docking of bFGF to FGFR1 in such a way that yielded a continuous stretch of heparin binding residues (purple side chains) of ~60 Å that transverse both proteins. Also shown is the 13-monosaccharide model of low MW HS, as described in Figure 11, again positioned ~5 Å below the span of cationic residues for both proteins. This alignment of HS sites in the two proteins concomitantly juxtaposed the putative receptor binding β turn of bFGF, ^{110}KYTSW^{114} (Baird et al., 1988), represented by the red solvent-accessible surface area on the right, against the white solvent-accessible surface of FGFR1, essentially the protein A binding site of the homologous Fc fragment (Deisenhofer, 1981). It is composed of three loop regions that connect (1) A and B β strands in the D(II) domain, (2) E and F β strands in the D(II) domain, and (3) F and G β strands in the D(III) domain. The second solvent accessible surface area on the left (red) for bFGF was identified as another FGFR1 binding site by site-directed mutagenesis mapping (Springer et al., unpublished results), consistent with the binding stoichiometry of bFGF observed in the presence of HS (Figure 7).

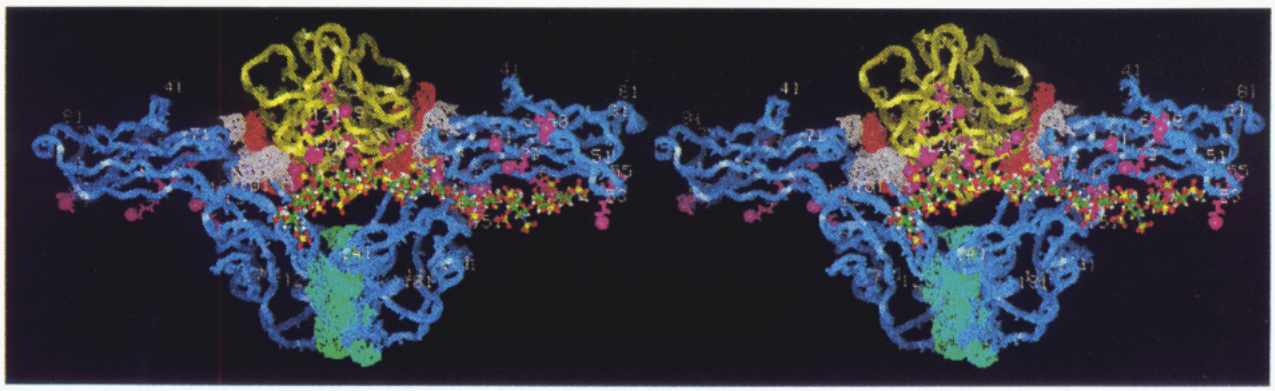

FIGURE 13: Structural model for the quaternary complex of FGFR1, bFGF, and HS. This three-dimensional structural model adds a second D(II)–D(III) FGFR1 moiety to the ternary complex of Figure 12 to reveal how the three reactants of the FGF system can be assembled to satisfy all of the multivalent binding results but still remain within the framework of the identified structural components of the X-ray structure of bFGF and the homology model of D(II)–D(III) FGFR1, described here and elsewhere. In accordance with the ITC results, the FGF is shown to be trivalent, binding two FGFR1s at the red solvent-accessible surfaces and one HS at the purple site (Thompson et al., 1994). FGFR1 is also shown to be trivalent, binding one FGF at the proposed growth factor binding site (white surface), binding one HS at the positive electrostatic locus identified in Figure 9, and binding one FGFR1 via a D(III) dimer interface (green surface). Similarly, low MW HS is shown to be bivalent, binding FGF and FGFR1. The stronger HS dependence for reaction 4 over reaction 1 suggests that the putative receptor binding loop ^{110}KYTSW^{114} (red surface of bFGF on the right) is the secondary receptor binding locus, site 2, characterized by $\alpha\beta\gamma K_{RR} = 1.9$ (±0.7) μM when HS is present at 1.5 equiv/bFGF. This supposition is supported by site-directed mutagenesis changes in the ^{110}KYTSW^{114} β turn of bFGF (Springer et al., unpublished results). When HS is present at 1.0 mM, it is probable that a second low MW HS binds to the other FGFR1 heparin binding site forming a quinary complex, as shown in Figure 10.

is consistent with all the experimental and structural results reported here: (1) the stoichiometry observed for the ITC experiments with a minimum of 1.5 equiv HS/bFGF; (2) equilibrium sedimentation data for $[FGFR1]_t/[bFGF]_t = 2.0$ in the presence of 1.0 mM HS; (3) the alignment of the continuous span of heparin binding residues for FGFR1 and bFGF; (4) the alignment of the putative receptor binding loop, ^{110}KYTSW^{114}, with the proposed FGF binding site of FGFR1; and (5) site-directed mutagenesis mapping of FGFR1 binding sites on bFGF to be reported elsewhere (Springer et al., unpublished results). Figure 13, therefore, shows a possible structural consequence of a trivalent bFGF, a trivalent D(II)–D(III) FGFR1, and a bivalent HS assembled in a data-driven manner.

The surfaces involved in bFGF/FGFR1 interactions are shown in Figure 13 as solvent-accessible surface areas calculated with a 1.4-Å water probe (Richards, 1977). Each of the receptor binding sites on bFGF (red surfaces) was found to be ~400 Å^2, indicating that the proposed growth factor binding site of FGFR1 (white surface) is also ~400 Å^2. The

dimer interface surface (green) located in the D(III) domain model was found to be ~650 Å^2 a piece. Therefore, the assembled model of Figure 13 predicts that ~2100 Å^2 of solvent-exposed protein residues become buried upon binding of the second FGFR1 to bFGF, which is similar to the 1900 Å^2 buried upon binding of the second receptor molecule to HGH (DeVos et al., 1992). A larger proportion of the predicted ~2100 Å^2 buried by the second FGFR1 binding event, however, was found to be apolar (~67%) than that observed for the HGH/HGH receptor (~51%). This finding is encouraging since such a large buried apolar surface area, ΔA_{apol} = −1400 Å^2, upon binding of the second receptor to bFGF would be consistent with the entropy dominated nature of this reaction (Table 3) if the enthalpy of binding, ΔH_2, is calculated by the methods of Murphy et al. (1993).

Finally, the assembled structural model of bFGF/HS-bridged FGF receptors in Figure 13, together with the mechanism proposed in Figure 10, was found useful for comprehending reports in the literature that heparin can be an agonist, promoting angiogenesis (Taylor & Folkman, 1982), or an antagonist, depending on circumstances (Folkman et al., 1983). Indeed, hexa- and octasaccharide-sized heparin fragments were reported to be antagonists of angiogenesis (Folkman et al., 1983) and bFGF-mediated proliferation of endothelial cells (Ishihara et al., 1993), while decasaccharide-sized or larger fragments of heparin were found to support bFGF-mediated mitogenesis (Ishihara et al., 1993). These results can be explained if FGFR dimerization is facilitated by a single heparin molecule of sufficient length (~60 Å) binding to both bFGF and FGFR (Figure 13), whereas, the smaller (~30 Å) hexasaccharide fragments will only be able to bind to either FGF or FGFR1 and thereby tie up one or the other in a nonproductive complex that precludes the second receptor binding event and consequently inhibits mitogenesis and angiogenesis. In this regard, the binding and structural results reported here may provide an opportunity to reevaluate the mechanism of action of many of the other known inhibitors of angiogenesis that are sulfated oligosaccharides, such as PPS (Lippman, 1993), SP-PG (Nakamura et al., 1992), or their nonsaccharide mimics, such as suramin (Harris et al., 1992), currently being examined for their therapeutic value in treating breast cancer and AIDS-related Kaposi sarcoma.

ACKNOWLEDGMENT

We thank Michael Levitt for introducing us to his segment match modeling program, SEGMOD, and for his assistance in the construction of the D(II)–D(III) FGFR1 model. We are grateful to Stephen Sprang and Doug Rees for providing their X-ray coordinates of basic and acidic FGF, respectively, and to Leo Thompson for many discussions about the heparin binding site of bFGF. We also thank Bill Herblin and Frank Barbera for the BHK assays; Gary Cooke and Sylvia Stack for their help in cloning, sequencing, and expression of bFGF and FGFR1; Ram Seetharam, Jeanne Corman, George Koukedis, and Shubi Kamerkar for N-terminal sequence and amino acid composition analysis; and Jodi Duke, Ann Yetter, and Joseph Pepe for assistance in protein recovery. Finally, we thank Pat Weber and Martin Thoolen for their encouragement and support.

REFERENCES

Ago, H., Kitagawa, Y., Fujishima, A., Matsuura, Y., & Katsube, Y. (1991) *J. Biochem. 110*, 360–363.

Arnott, S., & Mitra, A. K. (1984) in *Molecular Biophysics of the Extracellular Matrix* (Arnott, S., Rees, D. A., & Morris, E. R., Eds.) pp 41–67, Humana Press, Clifton, NJ.

Baird, A., Schubert, D., Ling, N., & Guillemin, R. (1988) *Proc. Natl. Acad. Sci. U.S.A. 85*, 2324–2328.

Bellot, F., Crumley, G., Kaplow, J. M., Schlessinger, J., Jaye, M., & Dionne, C. A. (1991) *EMBO J. 10*, 2849–2854.

Bergonzoni, L., Caccia, P., Cletini, O., Sarmientos, P., & Isacchi, A. (1992) *Eur. J. Biochem. 210*, 823–829.

Bode, W., Turk, D., & Karshikov, A. (1992) *Protein Sci. 1*, 426–471.

Brandts, J. F., & Jacobson, B. S. (1983) *Surv. Synth. Pathol. Res. 2*, 107–114.

Brandts, J. F., Lin, L.-N., Wiseman, T., Williston, S., & Yang, C. P. (1990) *Am. Lab. 22*, 30–41.

Brooks, I., Watts, D. G., Soneson, K. K., & Hensley, P. (1994) *Methods Enzymol.* (in press).

Burgess, W. H., & Maciag, T. (1989) *Annu. Rev. Biochem. 58*, 575–606.

Chauhan, A. K., Li, Y.-S., & Deuel, T. F. (1993) *Proc. Natl. Acad. Sci. U.S.A. 90*, 679–682.

Connelly, P. R., Varadarajan, R., Sturtevant, J. M., & Richards, F. M. (1990) *Biochemistry 29*, 6108–6114.

Cunningham, B. C., Ultsch, M., De Vos, A. M., Mulkerrin, M. G., Clauser, K. R., & Wells, J. A. (1991) *Science 254*, 821–825.

Deisenhofer, J. (1981) *Biochemistry 20*, 2361–2370.

Delli-Bovi, P., Curatola, A. M., Newman, K. M., Sato, Y., Moscatelli, D., Hewick, R. M., Rifkin, D. B., & Basilico, C. (1988) *Mol. Cell. Biol. 8*, 2933–2941.

De Vos, A. M., Ultsch, M., & Kossiakoff, A. A. (1992) *Science 255*, 306–312.

Dionne, C. A., Crumley, G., Bellot, F., Kaplow, J. M., Searfoss, G., Ruta, M., Burgess, W. H., Jaye, M., & Schlessinger, J. (1990) *EMBO J. 9*, 2685–2692.

Edman, P., & Begg, G. (1967) *Eur. J. Biochem. 1*, 80–91.

Eriksson, A. E., Cousens, L. S., Weaver, L. H., & Matthews, B. W. (1991) *Proc. Natl. Acad. Sci. U.S.A. 88*, 3441–3445.

Finch, P. W., Rubin, J. S., Miki, T., Ron, D., & Aaronson, S. A. (1989) *Science 245*, 752–755.

Folkman, J. (1985) *Adv. Cancer Res. 43*, 175–203.

Folkman, J., & Klagsbrun, M. (1987) *Science 235*, 442–447.

Folkman, J., & Shing, Y. (1992) *J. Biol. Chem. 267*, 10931–10934.

Folkman, J., Langer, R., Linhardt, R. J., Haudenschild, C., & Taylor, S. (1983) *Science 221*, 719–725.

Gallagher, J. T., & Turnbull, J. E. (1992) *Glycobiology 2*, 523–528.

Gilson, M., Sharp, K., & Honig, B. (1988) *J. Comput. Chem. 9*, 327–335.

Gospodarowicz, D., Cheng, J., Lui, G.-M., Baird, A., & Bohlen, P. (1984) *Proc. Natl. Acad. Sci. U.S.A. 81*, 6963–6967.

Gospodarowicz, D., Neufeld, G., & Schweigerer, L. (1986) *Mol. Cell. Endocrinol. 46*, 187–204.

Gospodarowicz, D., Ferrara, N., Schweigerer, L., & Neufeld, G. (1987) *Endocr. Rev. 8*, 95–114.

Grimes, J. K. (1985) in *Analytical Solution Calorimetry* (Grimes, J. K., Ed.) pp 299–390, Wiley & Sons, New York.

Grootenhuis, P. D. J., & van Boeckel, C. A. A. (1991) *J. Am. Chem. Soc. 113*, 2743–2747.

Harris, J. R., Lippman, M. E., Veronesi, U., & Willett, W. (1992) *N. Engl. J. Med. 327*, 473–480.

Higashiyama, S., Lau, K., Besner, G. E., Abraham, J. A., & Klagsbrun, M. (1992) *J. Biol. Chem. 267*, 6205–6212.

Horlick, R. A., Stack, S. L., & Cooke, G. M. (1992) *Gene 120*, 291–295.

Hou, J., Kan, M., McKeehan, K., McBride, G., Adams, P., & McKeehan, W. L. (1991) *Science 251*, 665–668.

Houssaint, E., Blanquet, P. R., Champion-Arnaud, P., Gesnel, M. C., Torriglia, A., Courtois, Y., & Breathnach, R. (1990) *Proc. Natl. Acad. Sci. U.S.A. 87*, 8180–8184.

Isacchi, A., Bergonzoni, L., & Sarmientos, P. (1990) *Nucleic Acids Res. 18*, 1906.

Ishihara, M., Tyrrell, D. J., Stauber, G. B., Brown, S., Cousens, L. S., & Stack, R. J. (1993) *J. Biol. Chem. 268*, 4675–4683.

Jaye, M., Schlessinger, J., & Dionne, C. A. (1992) *Biochim. Biophys. Acta 1135*, 185–199.
Johnson, D. E., Lee, P. L., Lu, J., & Williams, L. T. (1990) *Mol. Cell. Biol. 10*, 4728–4736.
Johnson, D. E., Lu, J., Chen, H., Werner, S., & Williams, L. T. (1991) *Mol. Cell. Biol. 11*, 4627–4634.
Kan, M., Wang, F., Xu, J., Crabb, J. W., Hou, J., & McKeehan, W. L. (1993) *Science 259*, 1918–1921.
Kiefer, M. C., Baird, A., Nguyen, T., George-Nascimento, C., Mason, O. B., Boley, L. J., Valenzuela, P., & Barr, P. J. (1991) *Growth Factors 5*, 115–127.
Klagsbrun, M., & Baird, A. (1991) *Cell 67*, 229–231.
Kuntz, I. D. (1992) *Science 257*, 1078–1082.
Laemmli, U. K. (1970) *Nature 227*, 680–695.
Leahy, D. J., Hendrickson, W. A., Aukhil, I., & Erickson, H. P. (1992) *Science 258*, 987–991.
Lee, P. L., Johnson, D. E., Cousens, L. S., Fried, V. A., & Williams, L. T. (1989) *Science 245*, 57–60.
Levitt, M. (1983) *J. Mol. Biol. 168*, 595–620.
Levitt, M. (1992) *J. Mol. Biol. 226*, 507–533.
Lin, L.-N., Mason, A. B., Woodworth, R. C., & Brandts, J. F. (1991) *Biochemistry 30*, 11660–11669.
Lippman, M. E. (1993) *Science 259*, 631–632.
Lobb, R. R., & Fett, J. W. (1984) *Biochemistry 23*, 6295–6299.
Luyten, F. P., Cunningham, N. S., Ma, S., Muthukumaran, N., Hammonds, R. G., Nevins, W. B., Wood, W. I., & Reddi, A. H. (1989) *J. Biol. Chem. 264*, 13377–13380.
Marics, I., Adelaide, J., Raybaud, F., Mattei, M. G., Coulier, F., Planche, J., de Lapeyriere, O., & Birnbaum, D. (1989) *Oncogene 4*, 335–340.
Marvizón, J.-C., & Baudry, M. (1993) *Anal. Biochem. 213*, 3–11.
Melnyk, V. O., Shipley, G. D., Sternfeld, M. D., Sherman, L., & Rosenbaum, J.T. (1990) *Arthritis Rheum. 33*, 493–500.
Miki, T., Bottaro, D. P., Fleming T. P., Smith, C. L., Burgess, W. H., Chan, A. M.-L., & Aaronson, S. A. (1992) *Proc. Natl. Acad. Sci. U.S.A. 89*, 246–250.
Mitra, A. K., Arnott, S., Atkins, E. D. T., & Isaac, D. H. (1983) *J. Mol. Biol. 169*, 873–901.
Moore, R., Casey, G., Brookes, S., Dixon, M., Peters, G., & Dickson, C. (1986) *EMBO J. 5*, 919–924.
Moscatelli, D. (1987) *J. Cell Physiol. 131*, 123–130.
Moses, M. A., & Langer, R. (1991) *Bio/Technology 9*, 630–634.
Murphy, K. P., Xie, D., Garcia, K. C., Amzel, L. M., & Freire, E. (1993) *Proteins: Struct., Funct., Genet. 15*, 113–120.
Nakamura, S., Sakurada, S., Salahuddin, S. Z., Osada, Y., Tanaka, N. G., Sakamoto, N., Sekiguchi, M., & Gallo, R. C. (1992) *Science 255*, 1437–1440.
Neufeld, G., & Gospodarowicz, D. (1985) *J. Biol. Chem. 260*, 13860–13868.
Nugent, M. A., & Edelman, E. R. (1992) *Biochemistry 31*, 8876–8883.
Olson, S. T., & Björk, I. (1991) *J. Biol. Chem. 266*, 6353–6364.
Olson, S. T., Halvorson, H. R., & Björk, I. (1991) *J. Biol. Chem. 266*, 6342–6352.
Ornitz, D. M., Yayon, A., Flanagan, J. G., Svahn, C. M., Levi, E., & Leder, P. (1992) *Mol. Cell. Biol. 12*, 240–247.
Pantoliano, M. W., Bird, R. E., Johnson, S., Asel, E. D., Dodd, S. W., Wood, J. F., & Hardman, K. D. (1991) *Biochemistry 30*, 10117–10125.
Partanen, J., Mäkelä, T. P., Eerola, E., Korhonen, J., Hirvonen, H., Claesson-Welsh, L., & Alitalo, K. (1991) *EMBO J. 10*, 1347–1354.
Pasquale, E. B. (1990) *Proc. Natl. Acad. Sci U.S.A. 87*, 5812–5816.
Pasquale, E. B., & Singer, S. J. (1989) *Proc. Natl. Acad. Sci. U.S.A. 86*, 5449–5453.
Petitou, M., Lormeau, J.-C., & Choay, J. (1991) *Nature 350* (Suppl.), 30–33.
Rapraeger, A. C., Krufka, A., & Olwin, B. B. (1991) *Science 252*, 1705–1708.
Richards, F. M. (1977) *Annu. Rev. Biophys. Bioeng. 6*, 151–176.
Roberts, R., Gallagher, J., Spooncer, E., Allen, T. D., Bloomfield, F., & Dexter, T. M. (1988) *Nature 332*, 376–378.
Sali, A., Matsumoto, R., McNeil, H. P., Karplus, M., & Stevens, R. L. (1993) *J. Biol. Chem. 268*, 9023–9034.
Sambrook, J., Fritsch, E. F., & Maniatis, T. (1989) *Molecular Cloning: A Laboratory Manual*, 2nd ed., Cold Spring Harbor Laboratory Press, Cold Spring Harbor, NY.
Sharpe, R. J., Arndt, K. A., Bauer, S. I., & Maione, T. E. (1989) *Arch. Dermatol. 125*, 1359–1362.
Sheriff, S., Silverton, E. W., Padlan, E. A., Cohen, G. H., Smith-Gill, S. J., Finzel, B. C., & Davies, D. R. (1987) *Proc. Natl. Acad. Sci. U.S.A. 84*, 8075–8079.
Shing, Y., Folkman, J., Sullivan, R., Butterfield, C., Murray, J., & Klagsbrun, M. (1984) *Science 223*, 1296–1299.
Sivalingam, A., Kenney, J., Brown, G. C., Benson, W. E., & Donoso, L. (1990) *Arch. Ophthalmol. 108*, 869–872.
Squires, C. H., Childs, J., Eisenberg, S. P., Polverini, P. J., & Sommer, A. (1988) *J. Biol. Chem. 263*, 16297–16302.
Stoddard, B. L., & Koshland, D. E. (1992) *Nature 358*, 774–776.
Summers, M. D., & Smith, G. E. (1987) *A Manual of Methods for Baculovirus Vectors and Insect Cell Culture Procedures*, Texas Agricultural Experimental Station Bulletin 1555, College Station, TX.
Taira, M., Yoshida, T., Miyagawa, K., Sakamoto, H., Terada, M., & Sugimura, T. (1987) *Proc. Natl. Acad. Sci. U.S.A. 84*, 2980–2984.
Tarentino, A. L., Gómez, C. M., & Plummer, T. H., Jr. (1985) *Biochemistry 24*, 4665–4671.
Taylor, S., & Folkman, J., (1982) *Nature 297*, 307.
Thompson, L. D., Pantoliano, M. W., & Springer, B. A. (1994) *Biochemistry 33*, 3831–3840.
Tyrrell, D. J., Ishihara, M., Rao, N., Horne, A., Kiefer, M. C., Stauber, G. B., Lam, L. H., & Stack, R. J. (1993) *J. Biol. Chem. 268*, 4684–4689.
Ueno, H., Gunn, M., Dell, K., Tseng, A., & Williams, L. (1992) *J. Biol. Chem. 267*, 1470–1476.
Ullrich, A., & Schlessinger, J. (1990) *Cell 61*, 203–212.
Vialard, J., Lalumiere, M., Vernet, T., Briedis, D., Alkhatib, G., Henning, D., Levin, D., & Richardson, C. (1990) *J. Virol. 64*, 37–50.
Weber, G. (1975) *Adv. Protein Chem. 29*, 1–83.
Weber, P. C., Wendoloski, J. J., Pantoliano, M. W., & Salemme, F. R. (1992) *J. Am. Chem. Soc. 114*, 3197–3200.
Weber, P. C., Pantoliano, M. W., Simons, D. M., & Salemme, F. R. (1994) *J. Am. Chem. Soc. 116*, 2717–2724.
Weiner, P. K., & Kollman, P. A. (1981) *J. Comput. Chem. 2*, 287–303.
Wellstein, A., Zugmaier, G., Califano, J. A., III, Kern, F., Paik, S., & Lippman, M. E. (1991) *J. Natl. Cancer Inst. 83*, 716–720.
Wiseman, T., Williston, S., Brandts, J. F., & Lin, L.-N. (1989) *Anal. Biochem. 179*, 131–137.
Wozney, J. M., Rosen, V., Celeste, A. J., Mitsock, L. M., Whitters, M. J., Kriz, R. W., Hewick, R. M., & Wang, E. A. (1988) *Science 242*, 1528–1534.
Wyman, J., Jr. (1964) *Adv. Protein Chem. 19*, 223–285.
Yanagishita, M., & Hascall, V. C. (1992) *J. Biol. Chem. 267*, 9451–9454.
Yayon, A., Klagsbrun, M., Esko, J. D., Leder, P., & Ornitz, D. M. (1991) *Cell 64*, 841–848.
Zhan, X., Bates, B., Hu, X., & Goldfarb, M. (1988) *Mol. Cell. Biol. 8*, 3487–3495.
Zhang, J., Cousens, L. S., Barr, P. J., & Sprang, S. R. (1991) *Proc. Natl. Acad. Sci. U.S.A. 88*, 3446–3450.
Zhu, X., Komiya, H., Chirino, A., Faham, S., Fox, G. M., Arakawa, T., Hsu, B.T., & Rees, D. C. (1991) *Science 251*, 90–93.
Zhu, X., Hsu, B. T., & Rees, D. C. (1993) *Structure 1*, 27–34.